Bull Volcanol (2007) 69: 301–318
DOI 10.1007/s00445-006-0075-4

RESEARCH ARTICLE

J. B. Witter · S. Self

The Kuwae (Vanuatu) eruption of AD 1452: potential magnitude and volatile release

Received: 24 March 2005 / Accepted: 24 March 2006 / Published online: 24 May 2006

Abstract Sometime during AD 1452, according to new evidence, a large-magnitude, initially phreatomagmatic eruption, destroyed the island of Kuwae (16.83°S, 168.54°E), located in the present-day Republic of Vanuatu. It created a 12×6-km submarine caldera composed of two adjacent basins. Based on estimates of caldera volume, between 30 and 60 km^3 DRE of dacite magma was ejected as pyroclastic flow and fall deposits during this event. Annual layers of ice dating from the period AD 1450–1460 contain acidity peaks representing fallout of sulfuric acid onto both the Greenland and Antarctic ice caps. These acidity peaks have been attributed by others to the sedimentation of H_2SO_4 aerosols that originated from sulfur degassing during the Kuwae eruption. Improved dating techniques and new data from nineteen ice cores reveal a single acidity peak attributed to Kuwae lasting from 1453 to 1457. In this study, we present new electron microprobe analyses of the S, Cl, and F contents of matrix glasses and glass inclusions in phenocrysts from tephra ejected during the Kuwae eruption. We establish that the Kuwae event did indeed yield a large release of sulfur gases. From our glass inclusion data and analysis, we calculate that the total atmospheric aerosol loading from the 1452 Kuwae eruption was ≫100 Tg H_2SO_4. Much of the volatile mass released during the eruption was probably contained in a separate, volatile-rich, fluid phase within the pre-eruptive Kuwae magma body. Comparing the volatile release of the Kuwae eruption with other large-magnitude eruptions, places Kuwae as the greatest sulfuric acid aerosol producer in the last seven centuries, larger even than sulfur emissions from the eruption of Tambora (Indonesia) in 1815, and possibly Laki (Iceland) in 1783. The severe and unusual climatic effects reported in the mid- to late-1450s were likely caused by the Kuwae eruption.

Keywords Volatile emissions · Caldera-forming eruption · Vanuatu · Sulfate aerosols · Ice cores · Kuwae · Fifteenth century

Editorial responsibility: J Stix

J. B. Witter (✉)
Hawaii Institute of Geophysics and Planetology,
University of Hawaii at Manoa,
1680 East West Road, POST 504,
Honolulu, HI 96822, USA
e-mail: witt_98103@yahoo.com

S. Self
Department of Earth Sciences, The Open University,
Walton Hall,
Milton Keynes, MK7 6AA, UK
e-mail: stephen.self@open.ac.uk

Present address:
J. B. Witter
ARKeX Limited, Newton House,
Cambridge Business Park, Cowley Road,
Cambridge, CB4 0WZ, UK

Introduction

A local legend in Vanuatu (SW Pacific) describes a tremendous volcanic cataclysm that destroyed the large island of Kuwae (16.83°S, 168.54°E). This great volcanic event occurred sometime in the mid-fifteenth century AD and formed the 12×6 km Kuwae submarine caldera (Fig. 1), now separating the islands of Epi and Tongoa, in the present-day Republic of Vanuatu (see Monzier et al. 1994; Robin et al. 1994b and references therein). The Kuwae eruption is believed to have generated a significant aerosol cloud, distributed in both hemispheres, based on acidity data from polar ice cores (Delmas et al. 1992; Zielinski 1995). Large caldera-forming eruptions such as Kuwae, often have a significant, but short-term, impact on Earth's climate. Reports of severe weather, unusual atmospheric optical effects (Pang 1993), and anomalously low tree ring densities from this period, suggesting cool summer conditions (Briffa et al. 1998), have also been tentatively attributed to a AD 1452 eruption of Kuwae.

Explosive volcanic eruptions impact climate by injecting sulfur (S) gases into the stratosphere, followed by conversion of these gases into H_2SO_4 (sulfate) aerosols which absorb incoming radiation causing stratospheric heating and tropospheric cooling (e.g., McCormick et al. 1995;

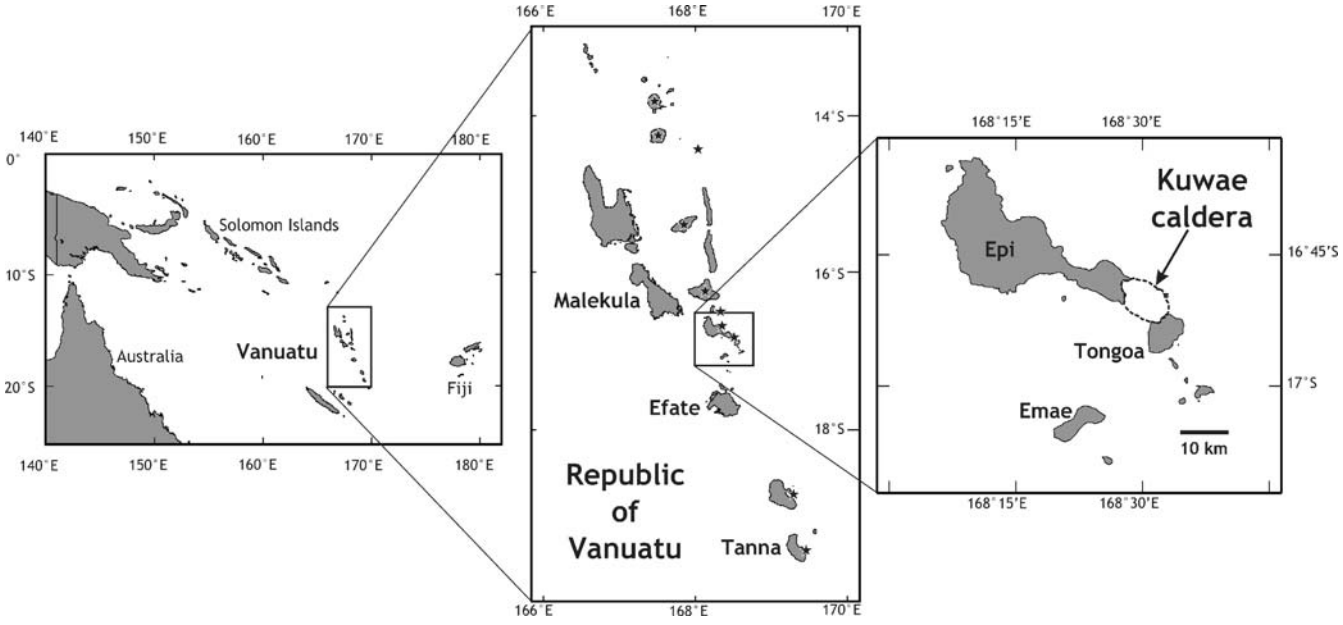

Fig. 1 Kuwae submarine caldera located in the central portion of the Republic of Vanuatu in the southwest Pacific. *Stars* denote island volcanoes that have erupted in the last five centuries

Robock 2000). The main purpose of the present study is to examine, on petrological grounds (Devine et al. 1984; Sharma et al. 2004), whether the Kuwae eruption could have been a large producer of S gases and, thus sulfate aerosols. We present results of major-element and volatile (S, Cl, F) analyses of glass inclusions and matrix glasses in tephra from the Kuwae eruption and consider a variety of scenarios to estimate total volatile emission. We also assess S output by comparison with eruptions of arc magmas that may harbor a co-existing, pre-eruptive, volatile-rich fluid phase , so-called "excess sulfur" (e.g., Scaillet et al. 2003).

Together with the results of a companion study of bi-polar ice-core acidity records in the 1450s (Gao et al. 2006), this work strongly suggests that the Kuwae eruption was responsible for the unusual climatic and optical effects recorded in the 1450s. Our companion ice-core study

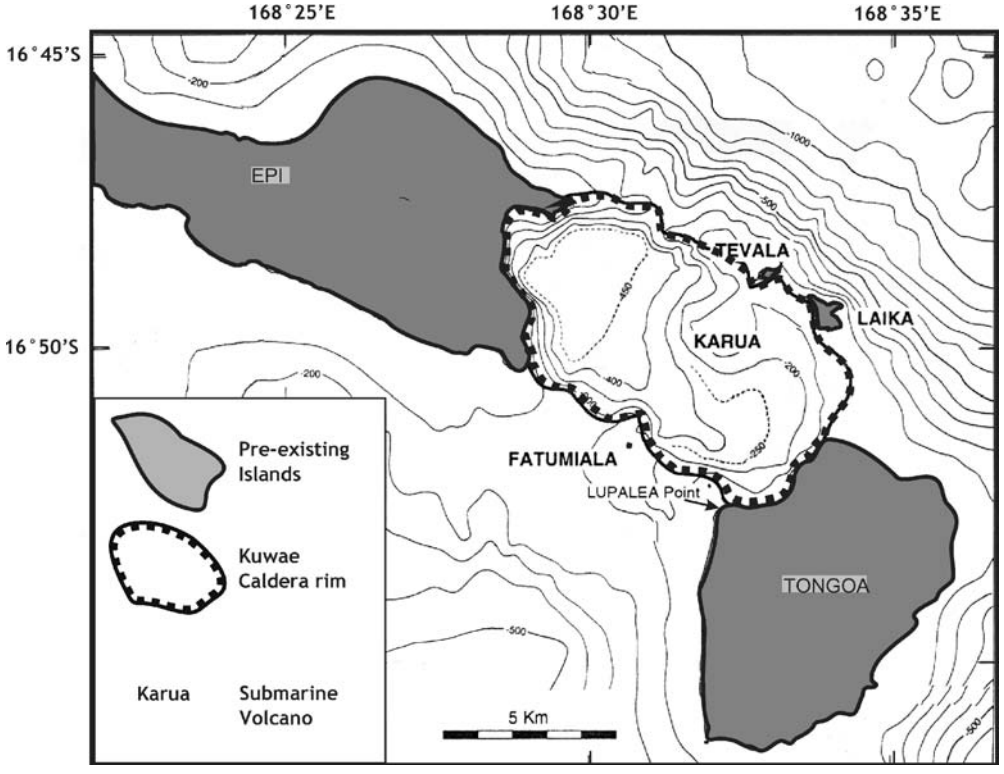

Fig. 2 Kuwae submarine caldera is bounded by the islands of Epi and Tongoa as well as the islets of Laika, Tevala, and Fatumiala Rock. Kuwae Caldera consists of NW and SE basins, ~450 and ~250 m deep, respectively. Bathymetric contour interval is 100 m. Adapted from bathymetric map from R/V Alis cruises of 1991 and 1992, published in Monzier et al. (1994)

indicates that the eruption year was 1452 and that it was followed by a major global aerosol event lasting from 1453 to 1457. This was one of the greatest atmospheric aerosol clouds of the last 1,000 years, probably even exceeding in mass that caused by the eruption of Tambora in 1815 but smaller than an aerosol mass reported ~1258–9 AD (Oppenheimer 2003).

Geologic setting of Kuwae caldera

Kuwae submarine caldera is located in the SW Pacific in the central portion of the New Hebrides island arc (Fig. 1). The 12×6 km diameter caldera is flanked by the islands of Epi and Tongoa to the NW and SE respectively, as well as the islets of Tevala and Laika to the NE, and Fatumiala Rock to the south (Fig. 2). The greatest vertical relief on the subaerial caldera wall is ~210 m on Tongoa. The caldera is composed of two coalesced, basin-like collapse structures (Robin et al. 1994b). The basin to the NW is the deeper of the two at ~450 m while the SE basin reaches ~250 m water depth. Seismic reflection data (Crawford et al. 1988) suggests that the intra-caldera deposits may be up to 380 m thick. Thus, total caldera subsidence during the caldera-forming event may have been as great as 800–1,100 m (Monzier et al. 1994), similar to more recent caldera collapse events such as at Tambora (Indonesia) in 1815 (>1,000 m; Petrochevsky 1949). The two basins are separated by the active Karua submarine volcano, a predominantly basaltic cone ~1 km^3 in volume that last erupted in 1974 forming a small ephemeral island. Monzier et al. (1994) calculated that the Kuwae event yielded 32–39 km^3 DRE (dense rock equivalent) of magma based on caldera size and morphology. They assumed that both basins formed during the mid-fifteenth century cataclysm. The errors on this estimate are not given by the authors but may be significant.

Much of Tongoa and Epi islands are thickly blanketed with tephra (primarily ignimbrite) from the Kuwae eruption. However, detailed field mapping of the deposits, granulometric studies, and volume calculations based on field data have not been possible because the majority of the Kuwae eruptive products were deposited into the sea and exposure on the islands (apart from the caldera walls) is poor.

The regional geology of the Kuwae area suggests that small-volume mafic eruptions dominate volcanism in central Vanuatu, as is common throughout the New Hebrides island arc (Barsdell and Berry 1990; Crawford et al. 1988; Eggins 1993; Robin et al. 1993–1995). The islands of Tongoa and Epi are littered with monogenetic and polygenetic basalt to basaltic andesite scoria cones. Crustal fractures, due to tectonic segmentation of the New Hebrides arc (Taylor et al. 1995), may have provided pathways for the ascent and eruption of mafic magma to form these cones. Indeed, the products of the Kuwae eruption are underlain by a thick pre-caldera succession of thin, basalt to basaltic andesite lavas, intercalated with beds of mafic scoria, exposed in the caldera walls on Tongoa and Epi. Exposures of 5–20-m-thick sections of yellow, palagonitized, planar to wavy-bedded, phreatomagmatic tephra are also present. Monzier et al. (1994) postulated that the pre-eruption morphology of the Kuwae landmass was much like present-day Tongoa, consisting of an undulating landscape of numerous scoria cones with two larger polygenetic volcanoes, centered above the NW and SE basins of the present caldera. They suggest that these polygenetic cones were the source vents for the many lava flows now exposed in the caldera walls.

Eruption sequence and stratigraphy

The volcanic stratigraphy of the 1452 Kuwae eruption, the last major event from this volcanic system and therefore the uppermost deposits, was first deduced by Monzier et al. (1994) and Robin et al. (1994b) from various exposures on Tongoa and Laika, and in this study we follow their scheme. Interpretation of the Kuwae stratigraphy was further investigated during fieldwork conducted on Tongoa by the first author in 1996. The eruption commenced with a magmatic to phreatomagmatic explosive phase depositing basaltic andesite scoria fall and surge beds. These pre-climatic strombolian to surtseyan-style eruptions appear to have occurred for some time (months?) as intraformational gullying of the succession of scoria fall and surge beds is seen. Rapid erosion of the loose pyroclastic beds was probably due to tropical rainfall and/or ejection of water from the vent (cf. Rotognaio ash; Walker 1981; Smith and Houghton 1995). This period of mafic volcanism was immediately followed by a large-scale eruption of dacite magma, which included the deposition of a poorly vesiculated juvenile dacite and lithic-clast-rich ignimbrite lag breccia, as well as the volumetrically dominant non-welded dacite ignimbrite. The transition from low flux, wet/dry mafic volcanism to high flux, dry silicic volcanism is marked by a dacitic layer of phreatomagmatic origin (layer HD5 of Monzier et al. 1994). This first episode of dacite volcanism at Kuwae is thought to have resulted in the collapse of the southeastern basin (Monzier et al. 1994).

The next phase of the eruption produced another dacite phreatomagmatic layer (HD6 of Monzier et al. 1994), then large-scale eruptive activity continued with the deposition of thick dacitic welded ignimbrites now exposed on the island of Laika. This second episode of dacite volcanism is thought to have ended with the collapse of the northwestern basin (Robin et al. 1994b). Infilling of the SE basin by tephra from the NW vent is presumed to be the reason for the difference in depth between the two basins.

For this study, samples of juvenile pyroclastic material were taken from the lower scoria fall deposits, the lag breccia, and non-welded ignimbrite deposits found in a sea cliff exposure at Lupalea Point on the island of Tongoa. These deposits represent the initial mafic outburst as well as the first half of the climactic, ignimbrite-forming Kuwae eruption. We assume our suite of samples is representative of both the mafic and silicic portions of the eruption products. However, it is important to mention that the eruption of the initial mafic magma at Kuwae was volumetrically minor, would not have involved high

eruption columns and, therefore, is interpreted as not having contributed to injection of S gas at stratospheric altitudes.

Eruption timing and possible magnitude

Determining a precise date for the Kuwae eruption was initially challenging. Radiocarbon dating of carbonized logs in the ignimbrite, as well as collagen age dating of the body of local Chief Ti Tongoa Liseiriki, who led post-eruption resettlement, suggested an early-fifteenth century date (Monzier et al. 1994). Northern hemisphere tree-ring density studies by Briffa et al. (1998) supported a 1452 date for the eruption, based on an interpreted, anomalously cold year in 1453. Moreover, unusually severe weather and atmospheric optical effects were reported in China and Turkey in the early 1450s (Pang 1993; Simarski 1996). However, ice core acidity peaks, attributed to the Kuwae eruption, were given dates ranging from the late 1440's to the early 1460s. Our recent study of mid-fifteenth century ice core acidity peaks reveals a four-year-long, high acidity signal centered in the mid-1450s (Gao et al. 2006). This finding suggests that the climactic part of the Kuwae eruption yielded a short-lived atmospheric gas release, as the acidity records are interpreted as containing only a single major peak. Other contributing evidence comes from unpublished trace element data (J-P Eissen, 1996, personal communication), suggesting that the entire succession of welded and non-welded dacite ignimbrites were erupted from the same silicic magma body (Robin et al. 1994b). Furthermore, Monzier et al. (1994) reported finding no soil between the tephra layers that separate the first and second ignimbrite-forming dacitic phases of the eruption in outcrops in the caldera walls. From this lack of soil they inferred there was no significant time-break between the eruptions that formed the NW and SE basins. In summary, current evidence suggests that the entire Kuwae caldera likely formed in one continuous eruptive event in 1452.

There is little evidence, other than caldera-size, on which to base an eruptive magnitude estimate, and the existing volume estimate is 32–39 km^3 (Monzier et al. 1994). This value is probably a minimum and places Kuwae in the same size range as the deposits produced from Tambora in 1815 (30–33 km^3; Self et al. 2004), or slightly larger. We note that essentially two Tambora-size calderas (~6 km diameter) are proposed to have formed. Unfortunately, in the complete absence of data on deposit thickness distribution, we cannot make a firm estimate of magnitude but attempt below to place it within reasonable bounds.

A crude upper limit for the Kuwae magnitude would be twice Tambora's volume, or ~60 km^3. In attempting to propose a possible caldera size for the unknown AD 1257 eruption, Oppenheimer (2003) used an empirical relationship between eruptive mass and caldera diameter. This relationship, adapted to fit the accepted volumes (masses) and known caldera diameters of the Tambora, Krakatau, and Pinatubo island-arc eruptions, suggests that the Kuwae caldera (diameter of a circle of equal area 8.7 km) could be the result of a 1.3×10^{14} kg magma release (~52 km^3), in rough agreement with the 2x Tambora estimate. We also re-assessed the caldera volume and note that it could possibly range from 23–56 km^3, depending on estimated values for collapse diameter, intra-caldera fill depth, and the volume of the volcanic edifice(s) engulfed during the cataclysm.

In light of the above considerations, we will use a range of 30–60 km^3 magma volume for the Kuwae eruption in later calculations. This is equivalent to 7.5×10^{13} to 1.5×10^{14} kg at an appropriate density for the dacite magma of 2,500 kg m^{-3}, or a magnitude M6.9–7.2 (Mason et al. 2004). We also assume that this mass is dominantly dacite, and that any mafic magma ejected in the climactic phases formed a subordinate, but indeterminable, proportion.

The Kuwae eruption record in ice cores

In a companion study of polar ice core records from both hemispheres containing acidity signals attributed to the fifteenth century eruption of Kuwae (Gao et al. 2006), we have shown that there is a single, bi-hemisheric, long-lasting signal from 1453–1457, found in nineteen ice cores from both hemispheres signifying that the eruption occurred in 1452. Although the Northern Hemisphere (NH) and Southern Hemisphere (SH) polar acidity concentrations vary spatially on each ice-cap, aerosol fallout caused average acid (sulfate) deposition of 45 and 98 kg km^{-2} in Greenland and Antarctica, respectively. One conclusion from Gao et al. (2006) is that extrapolating from individual or group values of ice acidity concentrations to global aerosol burdens (cf. Delmas et al. 1992; Zielinski 1995) does not yield reliable estimates. However, what can be determined is the ratio of acid deposition from one eruption to another in the two polar ice-caps; for example, the average 1816 Tambora deposition was 50 kg km^{-2} over Greenland but only 59 kg km^{-2} over Antarctica. This result suggests that the total global aerosol cloud from Kuwae had a greater mass than that generated by Tambora, but the data cannot be extrapolated to global amounts, nor to determining a ratio between the total Tambora and Kuwae aerosol masses. We also determined that the Kuwae acid deposition was proportioned differently in each hemisphere (SH≈2×NH) to that of Tambora (SH≈NH). This may reflect the more southerly location of Kuwae (17 vs. 8°S) and, possibly, a different atmospheric circulation regime in 1815 compared to that in 1452 (Gao et al. 2006).

The long duration of the ice core acidity signal attributed to Kuwae (4 years; Gao et al. 2006) is indicative of a considerable aerosol mass (~100 Tg). Large injections of volcanic SO_2 may have caused stratospheric dehydration (Bekki 1995; Bekki et al. 1996; Savarino et al. 2003), which would have delayed conversion of SO_2 to sulfate thus lengthening the duration over which aerosols formed. Moreover, the Tambora eruption's aerosol cloud, estimated to have had a mass between 90 and 118 Tg (55–58 Tg SO_2; Self et al. 2004), serves as a useful comparison for the Kuwae case.

1452 Kuwae eruption deposits: sample descriptions

Scoria fall deposit Individual clasts and a bulk sample were collected from the lowermost scoria fall deposit of the 1452 succession at Lupalea Point (labeled KUWSF in the data tables; referred to as SF in the text for simplicity). This unit is made up of black, well-vesiculated, scoria clasts ~1–10 cm in diameter, in a matrix of palagonitized yellow ash.

Dacitic ignimbrite Juvenile blocks were collected from the lag breccia deposit (labeled KUWJLB in data tables; simply JLB in text) that overlies the scoria fall deposits and underlies the non-welded pyroclastic flow deposits at Lupalea Point. This deposit is rich in large (up to 30 cm) poorly vesiculated bombs in a fines-depleted matrix. The outer surfaces of these bombs are distinctly yellow while the interiors are black and glassy. Clasts of pumice and bulk deposit samples were also collected from the massive, poorly sorted (fines-rich), pumice-and lithic-rich, non-welded pyroclastic flow deposit (labeled KUWPFD in data tables; simply PFD in text) outcropping at Lupalea Point. The pumices in this deposit are 1–8 cm in diameter, buff in color and well-vesiculated.

Analytical methods

Minerals, matrix glasses, and glass inclusions in phenocrysts were analyzed for major-elements, and the glasses for sulfur, chlorine, and fluorine, at the University of Hawaii on a fully automated, wavelength-dispersive, five-spectrometer, Cameca SX-50 electron microprobe. All mineral analyses were conducted at 15 kV accelerating voltage, 15 nA beam current, and 1 μm beam diameter. Major-element glass analyses were performed at 15 kV accelerating voltage, 10 nA beam current, and 5 μm beam diameter. For glass analyses, a counting time of 30 s was used for the elements Si, Ti, Al, Fe, Mg, Ca, and K, 20 s for Na, 80 s for Mn, and 100 s for P. Na was analyzed using a PC0 diffraction crystal instead of TAP. Precision (1σ) for major elements is estimated at <1% for Si, Al, and Na; <2% for Fe, Mg, Ca, K, and P; <3% for Ti; and <5% for Mn, based on counting statistics.

Volatile elements S, Cl, and F were analyzed in glasses using the CSIRO-trace routine of Robinson and Graham (1992) with 15 kV accelerating voltage, 60 nA beam current, 5 μm focused beam, and a counting time of 400 s. Analytical precision (1σ) based on counting statistics for volatile elements are: S=±20 ppm, Cl=±16 ppm and F=± 80 ppm. Troilite, Scapolite, and Apatite were used as primary standards for S, Cl, and F, respectively. The glass standards VG2 and A99 were used as secondary standards and analyzed as unknowns for S, Cl, and F during each analytical session. The S, Cl, and F values for both secondary standards obtained in this study are in agreement with those of Thordarson et al. (1996; see Table 1). The concentration of H_2O in the analyzed glass inclusions was estimated using the difference technique (100 wt%–analytical total of major and volatile elements; Anderson 1974; Sisson and Layne 1993; Devine et al. 1995). While this method may give crude estimates, the results obtained are generally comparable with values determined using other techniques, and are deemed reasonable.

Major element oxides in whole rock samples were analyzed at the University of Hawaii by X-ray fluorescence (XRF) using a fully automated, wavelength-dispersive Siemens SRS 303 AS instrument with an Rh target X-ray tube, following the method of Norrish and Hutton (1969). Major element oxide abundances in the matrix glass of the dacite pumices from Kuwae were also analyzed by Activation Laboratories in Ancaster, Ontario, Canada by ICP-MS. The bulk sulfur concentration in the dacite pumice matrix glass was obtained by LECO analysis, performed by Activation Labs.

Results

For a more complete description of the mineralogy and petrology of Kuwae tephra see Witter (1997). Relevant aspects of that study are summarized here.

Whole-rock chemistry and mineralogy

Whole rock, major-element compositions of scoria and pumice are shown in Table 2. Samples SF and PFD are basaltic andesite and dacite, respectively, according to the classification system of LeBas et al. (1986). Published whole-rock analyses of similar rock samples from Robin et al. (1994b) are included in Table 2. Robin et al.'s whole-rock analysis of a dense juvenile block from layer HD5 (dacite) is analogous to our sample JLB based on stratigraphic position and texture.

Modal mineralogy and vesicularity were estimated by point counting ~1,000 points per thin section (Table 3). Phenocryst phases in the basaltic andesite (SF) in order of decreasing abundance are: plagioclase, olivine, magnetite, ± clinopyroxene. SF has a vesicle-free phenocryst content of

Table 1 Representative microprobe analyses of international standards using the CSIRO trace routine

VG2	S	Cl	F	n
Reported[a]	1365	316	300	139
SD	29	19	72	
This study	1331	295	219	8
SD	23	16	77	
A99	S	Cl	F	N
Reported[a]	220	227	765	42
SD	12	20	79	
This study	200	224	583	8
SD	15	16	82	

SD = standard deviation (1σ)
N = number of analyses
[a]Values reported by Thordarson et al. (1996)

Table 2 Whole-rock XRF analyses from this study as well as whole-rock analyses of similar samples from Robin et al. (1994b)

Label	KUWSF	HD1-T2C	HD5-T2J	KUWPFD	PFD2-T2N	PFD1-T4A	PFD2-T4B
Ref.	This study	Robin et al. 1994b	Robin et al.	This study	Robin et al.	Robin et al.	Robin et al.
SiO_2	52.39	51.92	64.33	63.05	62.49	64.43	63.91
TiO_2	0.89	0.83	0.60	0.62	0.61	0.60	0.61
Al_2O_3	18.17	18.31	15.37	17.06	16.00	15.53	15.61
FeO*[b]	11.07	10.45	6.35	6.46	6.69	6.25	6.28
MnO	0.19	0.19	0.15	0.15	0.16	0.15	0.15
MgO	3.94	3.87	1.71	1.65	2.05	1.68	1.78
CaO	9.76	9.86	4.80	5.11	5.73	4.80	5.04
Na_2O	2.26	2.99	3.93	3.43	3.77	3.80	3.91
K_2O	1.07	1.28	2.51	2.24	2.27	2.50	2.47
P_2O_5	0.26	0.30	0.24	0.22	0.23	0.25	0.24
Total[a]	100.00	100.00	99.99	100.00	100.00	99.99	100.00

Sample HD5-T2J is representative of our sample KUWJLB
[a]Oxide values have been recalculated to 100%
[b]Total Fe as FeO*

20 vol.% and a vesicularity of 63%. Phenocryst phases in the dacite samples (JLB and PFD) in order of decreasing abundance are: plagioclase, clinopyroxene, magnetite, orthopyroxene, ± olivine, ± rare sulfide. The juvenile bomb from the lag breccia (JLB) and the pumice from the pyroclastic flow deposit (PFD) are mineralogically very similar, although the lag breccia clast is much less vesicular than the pumice (30% vs. 64% vesicularity) and has a slightly lower vesicle-free phenocryst content (11 vs. 13 vol.%).

Plagioclase

Plagioclase phenocrysts in the dacite samples (JLB and PFD) commonly have normal, reverse, and oscillatory zonation. Many crystals have large embayments, sieve-textured interiors, and/or are riddled with glass inclusions. Some crystals are fractured while most are subhedral to anhedral; compositions span the range $An_{51–92}$. Plagioclase phenocrysts in the basaltic andesite sample (SF) are similar to those in the dacite, having variable zonation, large embayments, and many glass inclusions. However, the compositional range is more limited at $An_{72–86}$.

Pyroxene

Clinopyroxene phenocrysts in the dacite samples (JLB and PFD) are reverse, normal, and oscillatory zoned and have compositions that cover the range $Wo_{39–49}$ $En_{40–49}$ $Fs_{3–19}$. Orthopyroxene phenocrysts occur only in the dacite samples; compositions have the range $Wo_{3–4}$ $En_{64–69}$ $Fs_{28–32}$. Most orthopyroxene crystals have reverse zonation from core-to-rim. Clinopyroxene phenocrysts in the basaltic andesite (SF) are unzoned and have the composition Wo_{45} En_{47} Fs_{8}.

Olivine

Olivine phenocrysts were not observed in the dacite lag breccia (JLB) samples and are rare in the dacite pumice (PFD) where they are euhedral, unaltered, unzoned and have the composition $Fo_{71–74}$. Olivine phenocrysts from the basaltic andesite scoria (SF) have compositions ranging from $Fo_{74–76}$ and also lack zonation.

Table 3 Modal analyses of representative samples in vol.% based on 1,000 points per thin section

Sample	Deposit	Plag	Cpx	Opx	Ol	Mgt	Sulfide	Σ xls	Grndmss	Ves	Σ xls ves free
KUWPFD	Pyroclastic flow	3.3	0.9	0.2	<0.1	0.4	<0.1	4.8	31.6	63.6	13.2
KUWJLB	Juvenile lag breccia	5.1	1.3	0.3	0	0.6	<0.1	7.3	62.5	30.2	10.5
KUWSF	Scoria fall	7	<0.1	0	0.2	<0.1	0	7.2	29.6	63.2	19.6

Plag plagioclase; *Cpx* clinopyroxene; *Opx* orthopyroxene; *Ol* olivine; *Mgt* magnetite; *Σ xls* total
Vol.% crystals; *Grndmss* groundmass (matrix glass and minerals <0.05 mm); *Ves* vesicles; *Σ xls ves free* total vol.% crystals on a vesicle-free basis, i.e., Σ xls/(Σ xls + grndmss)

Glass chemistry

Matrix glass

Twenty-four major-element and 23 volatile (S, Cl, F) analyses of matrix glass in Kuwae tephra were performed by electron microprobe (Figs. 3 and 4; Table 4). Each analysis represents a single point in the matrix glass. The dacite pumice and lag breccia samples (PFD and JLB) have matrix glasses which are also dacite in composition; 64–65 wt% SiO_2 and 65–67 wt% SiO_2, respectively (Fig. 3). The basaltic andesite scoria sample (SF) has basaltic andesite matrix glass (52–53 wt% SiO_2).

Average matrix glass volatile contents (±1σ) for dacite pumice (PFD) are: 232±26 ppm S, 1492±92 ppm Cl, 330±89 ppm F, and 0.4±0.2 wt% H_2O (*n*=8; Table 4). Sulfur analysis of PFD matrix glass by LECO yielded 310 ppm S; slightly higher than the microprobe result. Average matrix glass volatile contents (±1σ) for the dacite lag breccia (JLB) are: 234±33 ppm S, 1312±185 ppm Cl, 403±44 ppm F, and 0.2±0.4 wt% H_2O (*n*=12; Table 4), within error of those from the dacite pumice.

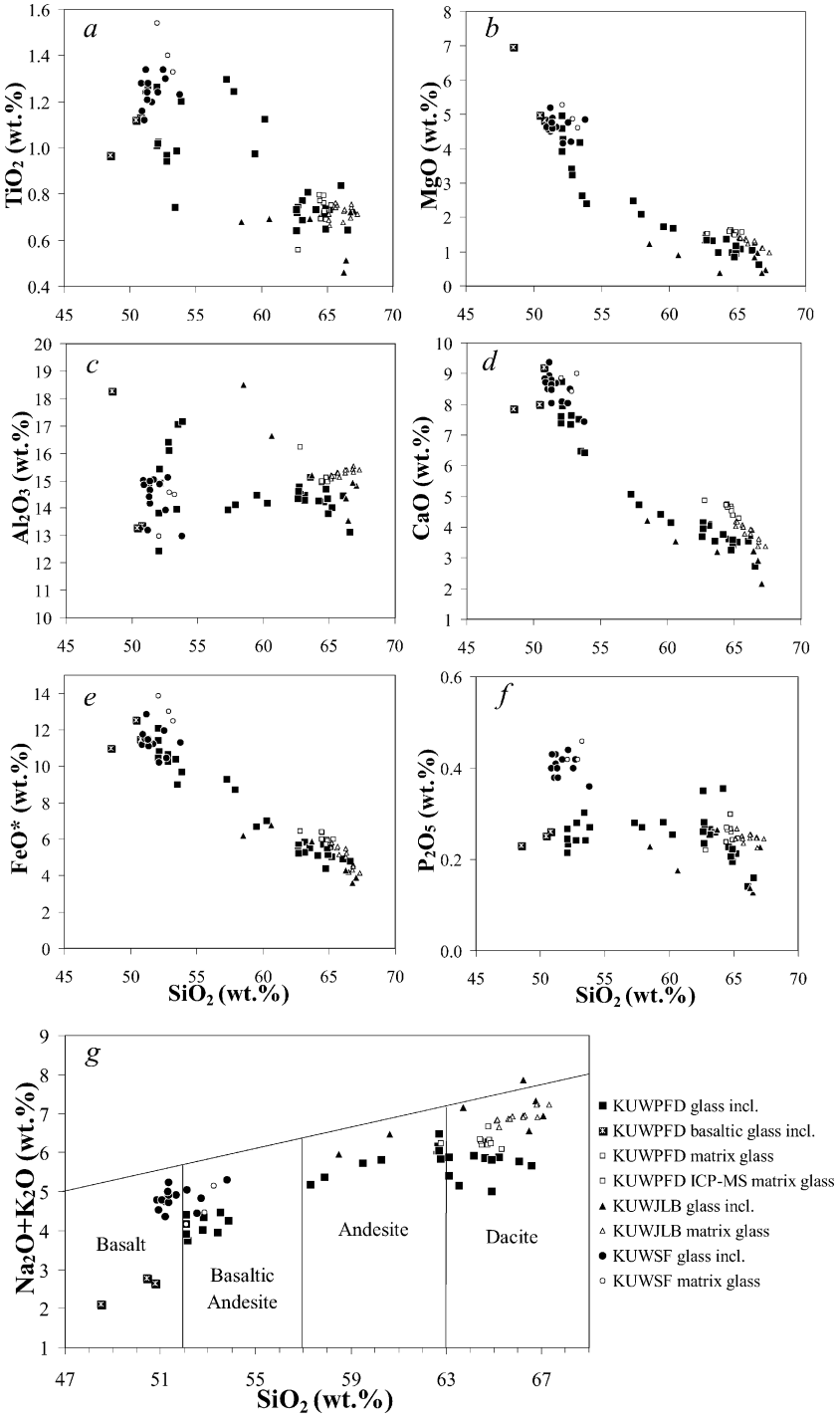

Fig. 3 SiO_2 vs. oxides. Compositional variations of SiO_2 vs. **a** TiO_2, **b** MgO, **c** Al_2O_3, **d** CaO, **e** FeO*, **f** P_2O_5, and **g** Na_2O+K_2O for glass inclusions in phenocrysts and matrix glasses from the basaltic andesite and dacite tephra from the eruption of Kuwae. All iron is reported as FeO*. Divisions in **g** are according to classification scheme of LeBas et al. (1986). Glass inclusions denoted by *black filled symbols*; matrix glasses by *open symbols*. Data from electron microprobe analyses of glass inclusions and matrix glass in samples of dacite pumice (KUWPFD, *squares*), dacite lag breccia (KUWJLB, *triangles*), and basaltic andesite scoria (KUWSF, *circles*) are shown. *Gray filled square* denotes results of ICP-MS analysis of a matrix glass separate from the dacite pumice (KUWPFD)

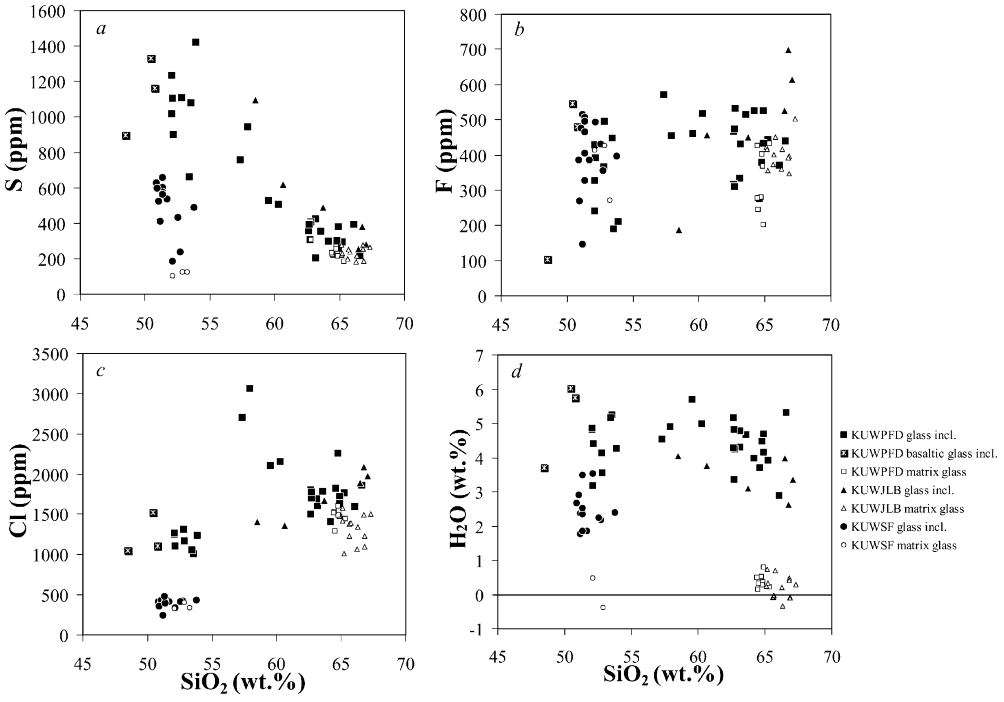

Fig. 4 Volatile content measured by electron microprobe in glass inclusions and matrix glasses plotted as SiO_2 vs. **a** Sulfur, **b**, Fluorine, **c** Chlorine, and **d** H_2O; H_2O concentrations estimated from electron microprobe data and determined by difference. Symbols as in Fig. 3. Analytical errors based on counting statistics are similar in size or smaller than the symbols for S, Cl, F, and SiO_2. Errors associated with calculating H_2O by difference from electron microprobe analyses are estimated at ±1.0 wt%

The matrix glass of the basaltic andesite sample (SF) has lower S and Cl contents (119±14 ppm S and 358±42 ppm Cl) than the dacite. SF matrix glass, and also contains 371±86 ppm F and <0.5 wt% H_2O (n=3; Table 4), results which are similar to those from the dacite.

Glass inclusions

Brown, black, and colorless glass inclusions up to 100 μm in maximum dimension are found in phenocrysts of plagioclase, clinopyroxene, orthopyroxene, and olivine, and are particularly abundant in plagioclase. Most glass inclusions average 20–40 μm across and are commonly elliptical in shape with the long axis of the inclusion parallel to mineral cleavage. Some glass inclusions contain small vapor bubbles (~5 μm) but these bubbles take up only a small proportion (<10%) of the inclusion. Most analyzed glass inclusions are small, such that only a single electron-microprobe analysis was made within each.

Thirty-nine major-element and 38 volatile-element analyses were performed on glass inclusions in phenocrysts in the dacite samples (PFD and JLB; Table 5). Glass inclusions found in phenocrysts in these samples cover a large compositional range from basalt to dacite (Fig. 3). Orthopyroxene phenocrysts contain only dacite glass inclusions while clinopyroxene phenocrysts contain dacite, andesite, and basaltic andesite glass inclusions. Glass inclusions found in plagioclase cover the entire compositional range from basalt to dacite. Olivine phenocrysts in the dacite contain basaltic glass inclusions (Fig. 5).

Fifteen major- and volatile-element analyses were performed on glass inclusions in plagioclase phenocrysts in basaltic andesite scoria (SF; Table 5). These range in composition from basalt to basaltic andesite (Fig. 3). One glass inclusion in olivine from SF yielded a basaltic andesite composition; however, an analytical total of 100 wt% suggests that it may be degassed or a re-entrant and may not accurately represent pre-eruptive magmatic compositions. As such, it was rejected from our dataset.

Major-element analyses of glass inclusions identify a wide variety of compositionally distinct silicate melts preserved in phenocrysts in Kuwae tephra. Dacite glass inclusions in the dacite pumice (PFD) are hosted by orthopyroxene, clinopyroxene, and plagioclase and have lower average silica and alkali contents and higher average MgO contents compared to dacite glass inclusions in clinopyroxene and plagioclase in the dacite lag breccia (JLB; Table 5, Fig. 5). Dacite glass inclusions in phenocrysts in the dacite pumice (PFD) average (±1σ): 332±68 ppm S, 1732±186 ppm Cl, 424±84 ppm F, and 4.3±0.6 wt% H_2O (n=16; Table 5, Fig. 6). Dacite glass inclusions in phenocrysts in the dacite lag breccia (JLB) have S, Cl, F, and H_2O contents (351±107 ppm S, 1908±174 ppm Cl, 573±107 ppm F, 3.3±0.6 wt% H_2O, n=4; Table 5, Fig. 6) that are within error of those in the dacite pumice (PFD). The glass inclusions in phenocrysts in the lag breccia clasts are slightly more evolved than those in the pumice, possibly due to a slower cooling regime. Regardless of the cause of these minor compositional differences, we contend that the dacite glass inclusions in phenocrysts in both the dacite pumice and lag breccia have their origins in the same dacite melt. It is also noted that the higher H_2O contents indicated by our data are similar to those obtained from experimental work on Pinatubo dacite (≤6 wt%, Scaillet and Evans 1999) at similar pressure and temperature conditions to those envisaged for the Kuwae dacite.

In contrast to dacite glass inclusions, andesite glass inclusions, hosted by plagioclase in PFD and clinopyrox-

Table 4 Electron microprobe analyses of matrix glasses in Kuwae tephra. All data reported as wt% oxides except S, Cl, and F which are reported in ppm

KUWPFD: Dacite pumice															
Label	SiO_2	TiO_2	Al_2O_3	Fe_2O_3	FeO	MnO	MgO	CaO	Na_2O	K_2O	P_2O_5	Total	S	Total	VDB
KUWPFD96[a]	62.75	0.56	16.23	0.39	6.10	0.14	1.53	4.87	3.95	2.29	0.22	99.03	310		
Label	SiO_2	TiO_2	Al_2O_3	FeO*	MnO	MgO	CaO	Na_2O	K_2O	P_2O_5	S	Cl	F	Total	VBD
kuw2mtrx1	64.73	0.76	15.10	5.82	0.17	1.50	4.68	3.53	2.68	0.30	270	1611	280	99.47	0.5
kuw2mtrx4	65.31	0.75	15.16	5.98	0.17	1.57	4.30	3.43	2.66	0.25	187	1444	433	99.78	0.2
kuw2mtrx5	64.80	0.73	15.01	6.01	0.16	1.53	4.60	3.57	2.76	0.26	244	1550	368	99.63	0.4
kuw2mtrx6	64.87	0.69	14.97	5.91	0.14	1.57	4.38	3.53	2.70	0.24	217	1474	203	99.19	0.8
kuw2mtrx7	64.75	0.79	15.13	5.70	0.14	1.50	4.54	3.86	2.81	0.27	257	1497	404	99.71	0.3
kuw1mtrx1	64.50	0.69	14.98	6.35	0.20	1.64	4.66	3.67	2.54	0.27	219	1300	246	99.67	0.3
kuw3mtrx1	64.43	0.77	14.92	6.42	0.13	1.64	4.76	3.68	2.63	0.27	227	1532	278	99.84	0.2
kuw3mtrx3	64.40	0.80	14.97	6.02	0.19	1.60	4.73	3.67	2.67	0.24	236	1525	426	99.49	0.5
Average	64.72	0.75	15.03	6.03	0.16	1.57	4.58	3.61	2.68	0.26	232	1492	330	99.60	0.4
1σ SD	0.30	0.04	0.09	0.25	0.02	0.06	0.16	0.13	0.08	0.02	26	92	89	0.21	0.2
KUWJLB: Juvenile dacite lag breccia															
Label	SiO_2	TiO_2	Al_2O_3	FeO*	MnO	MgO	CaO	Na_2O	K_2O	P_2O_5	S	Cl	F	Total	VBD
hd52mtrx1	65.12	0.71	15.21	5.68	0.18	1.40	4.18	4.08	2.73	0.25	277	1582	422	99.76	0.2
hd52mtrx2	65.14	0.69	15.07	5.56	0.13	1.39	4.01	4.11	2.72	0.25	219	1419	417	99.25	0.7
hd52mtrx3	67.31	0.71	15.39	4.13	0.13	0.98	3.38	4.13	3.08	0.25	265	1502	502	99.71	0.3
hd52mtrx4	66.84	0.74	15.53	4.57	0.15	1.10	3.51	4.25	3.00	0.25	186	1098	396	100.10	−0.1
hd52mtrx5	65.61	0.74	15.29	5.51	0.15	1.38	4.08	4.11	2.76	0.25	200	1382	373	100.08	−0.1
hd52mtrx6	66.25	0.73	15.30	5.03	0.11	1.26	3.79	4.10	2.85	0.25	184	1065	361	99.81	0.2
hd51mtrx1	65.21	0.66	15.19	5.78	0.19	1.40	4.17	3.90	2.74	0.27	230	1012	355	99.67	0.3
hd51mtrx2	65.77	0.75	15.12	5.13	0.12	1.24	3.78	4.10	2.84	0.24	239	1386	450	99.29	0.7
hd51mtrx3	65.67	0.76	15.28	5.58	0.14	1.33	3.99	4.09	2.76	0.25	250	1232	401	100.03	0.0
hd51mtrx4	66.79	0.70	15.43	4.31	0.11	1.11	3.37	4.27	2.96	0.25	277	1497	392	99.51	0.5
hd51mtrx5	66.24	0.68	15.38	5.47	0.13	1.31	3.93	4.15	2.76	0.25	NA	NA	NA	100.30	−0.3
hd51mtrx6	66.31	0.73	15.40	5.22	0.11	1.28	3.90	4.13	2.81	0.25	218	1346	417	100.33	−0.3
hd51mtrx7	66.82	0.75	15.32	4.50	0.15	1.11	3.62	4.15	2.76	0.23	257	1227	347	99.58	0.4
Average	66.08	0.72	15.30	5.11	0.14	1.25	3.82	4.12	2.83	0.25	234	1312	403	99.80	0.2
1σ SD	0.72	0.03	0.13	0.56	0.02	0.14	0.28	0.09	0.11	0.01	33	185	44	0.35	0.4
KUWSF: Basaltic Andesite Scoria															
Label	SiO_2	TiO_2	Al_2O_3	FeO*	MnO	MgO	CaO	Na_2O	K_2O	P_2O_5	S	Cl	F	Total	VBD
kuwsfmtrx1	53.23	1.33	14.50	12.47	0.19	4.61	9.00	3.35	1.81	0.46	127	340	272	101.02	−1.0
kuwsfmtrx2	52.08	1.54	12.99	13.85	0.25	5.28	8.87	2.07	2.09	0.42	103	329	414	99.52	0.5
kuwsfmtrx3	52.86	1.40	14.58	13.02	0.25	4.87	8.43	2.04	2.42	0.42	126	406	427	100.39	−0.4
Average	52.72	1.42	14.02	13.11	0.23	4.92	8.77	2.49	2.11	0.43	119	358	371	100.31	−0.3
1s SD	0.59	0.11	0.90	0.69	0.03	0.34	0.30	0.75	0.31	0.02	14	42	86	0.75	0.8

[a]Matrix glass of sample KUWPFD analyzed for major elements by ICP-MS, Fe_2O_3/FeO ratio by titration, and S by LECO at Activation Labs, Ancaster Ontario, Canada

*FeO** total iron. VBD (volatiles by difference) is calculated from 100 wt%−(sum of oxides and volatile elements)

NA not analyzed; *SD* standard deviation

ene in JLB, are highly variable in their volatile content. Plagioclase-hosted andesite glass inclusions in PFD average (±1σ) 685±207 ppm S, 2508±457 ppm Cl, 501±55 ppm F, and 5.0±0.5 wt% H_2O (n=4; Table 5, Fig. 6). Clinopyroxene-hosted andesite glass inclusions in JLB average (±1σ) 860±336 ppm S, 1389±33 ppm Cl, 322±191 ppm F, and 3.9±0.2 wt% H_2O (n=2; Table 5, Fig. 6). Our data suggests that there may be at least five andesite melts with compositionally distinct volatile contents preserved in glass inclusions in Kuwae dacite phenocrysts.

Basaltic andesite glass inclusions are found in clinopyroxene and plagioclase phenocrysts in PFD, and in plagioclase phenocrysts in SF. Silica contents are similar (53 wt% SiO_2) regardless of host phenocryst or bulk rock composition (Fig. 5), however, P_2O_5 is lower in glass inclusions in phenocrysts in PFD (0.26±0.03 wt% P_2O_5) compared with SF (0.41±0.03 wt% P_2O_5). In addition, except for fluorine, basaltic andesite glass inclusions in phenocrysts in PFD are more volatile-rich than those in SF (Fig. 6). Basaltic andesite glass inclusions in PFD average (±1σ) 1072±210 ppm S, 1187±108 ppm Cl, 345±110 ppm

Table 5 Electron microprobe analyses of glass inclusions in phenocrysts in Kuwae tephra

Label	Size (μm)	SiO_2	TiO_2	Al_2O_3	FeO*	MnO	MgO	CaO	Na_2O	K_2O	P_2O_5	S	Cl	F	Total	VBD
KUWPFD	Dacite glass inclusions in orthopyroxene host															
kuw3opx4inclb1	35×42	64.60	0.70	14.22	5.71	0.16	0.96	3.62	3.16	2.69	0.23	303	1824	275	96.29	3.7
kuw2opx25incla1	60×40	63.13	0.77	14.46	5.83	0.16	1.32	4.10	2.80	2.60	0.27	424	1607	432	95.68	4.3
	Average	63.87	0.73	14.34	5.77	0.16	1.14	3.86	2.98	2.65	0.25	364	1716	354	95.99	4.0
	1σ SD	1.04	0.05	0.17	0.09	0.00	0.25	0.33	0.26	0.06	0.03	86	153	111	0.43	0.4
KUWPFD	Dacite glass inclusions in clinopyroxene host															
kuw3cpx7incla1	73×65	65.20	0.73	14.00	5.03	0.17	1.08	3.52	3.09	2.79	0.21	295	1768	445	96.08	3.9
kuw3cpx7inclb1	53×54	64.90	0.65	13.80	5.17	0.15	0.96	3.43	3.02	2.79	0.22	262	1726	434	95.31	4.7
kuw3cpx7inclc1	24×20	66.57	0.65	13.13	4.80	0.11	0.62	2.73	2.69	2.96	0.16	215	1863	440	94.67	5.3
kuw3cpx7incld1	75×88	62.76	0.74	14.64	5.67	0.16	1.32	4.09	3.28	2.56	0.27	409	1752	533	95.75	4.2
kuw3cpx6incla1	40×100 irreg.	63.55	0.81	15.11	5.53	0.13	0.98	3.54	2.46	2.70	0.26	357	1791	516	95.33	4.7
kuw1cpx7incla	39×54	64.89	0.74	14.35	5.50	0.17	1.15	3.60	2.32	2.69	0.20	382	1633	527	95.84	4.2
kuw1cpx7inclc	30×20	66.06	0.84	14.44	4.92	0.14	1.03	3.54	3.06	2.70	0.14	394	1594	370	97.10	2.9
	Average	64.85	0.74	14.21	5.23	0.15	1.02	3.49	2.85	2.74	0.21	331	1732	466	95.72	4.3
	1σ SD	1.33	0.07	0.64	0.34	0.02	0.21	0.40	0.36	0.13	0.05	74	92	61	0.76	0.8
KUWPFD	Dacite glass inclusions in plagioclase host.															
kuw3plag10incla1	29×27	63.11	0.69	14.29	5.26	0.14	1.32	4.06	3.20	2.69	0.25	205	1692	334	95.23	4.8
kuw3plag2incla1	33×35	62.61	0.73	14.35	5.36	0.14	1.34	3.69	3.24	2.80	0.35	361	1500	468	94.84	5.2
kuw3plag2inclc1	45×45	62.70	0.72	14.76	5.66	0.13	1.50	4.17	3.81	2.67	0.28	309	1704	474	96.64	3.4
kuw3plag2incld1	45×30	64.16	0.73	14.27	5.11	0.12	1.35	3.77	3.20	2.71	0.36	299	1411	526	96.01	4.0
kuw2plag18incla1	25×20	64.78	0.72	14.68	4.38	0.13	0.84	3.24	3.19	3.07	0.21	304	2258	380	95.52	4.5
kuw1plag4incla1	53×74 irreg.	62.65	0.73	14.62	5.37	0.12	1.41	4.15	3.54	2.61	0.26	398	1803	316	95.70	4.3
kuw3plag3incla1	100×100 irreg.	62.68	0.64	14.62	5.22	0.18	1.34	3.95	3.28	2.78	0.24	396	1782	310	95.17	4.8
	Average	63.24	0.71	14.51	5.19	0.14	1.30	3.86	3.35	2.76	0.28	325	1736	401	95.59	4.4
	1σ SD	0.87	0.03	0.20	0.40	0.02	0.21	0.33	0.24	0.15	0.06	68	272	87	0.60	0.6
KUWPFD	Dacite glass inclusions in all host minerals.															
		SiO_2	TiO_2	Al_2O_3	FeO*	MnO	MgO	CaO	Na_2O	K_2O	P_2O_5	S	Cl	F	Total	VBD
	Average	64.02	0.72	14.36	5.28	0.15	1.16	3.70	3.08	2.74	0.24	332	1732	424	95.70	4.3
	1σ SD	1.30	0.05	0.45	0.38	0.02	0.24	0.39	0.37	0.13	0.06	68	186	84	0.64	0.6
KUWPFD	Andesite glass inclusions in plagioclase host.															
Label	size (μm)	SiO_2	TiO_2	Al_2O_3	FeO*	MnO	MgO	CaO	Na_2O	K_2O	P_2O_5	S	Cl	F	Total	VBD
kuw3plag2inclb1	40×30	59.52	0.97	14.48	6.69	0.19	1.73	4.41	3.20	2.52	0.28	529	2113	461	94.30	5.7
kuw3plag4incla1	22×9	60.28	1.12	14.17	7.00	0.20	1.68	4.16	3.09	2.73	0.25	508	2153	517	95.00	5.0
kuw3plag3inclb1	44×35	57.30	1.30	13.93	9.27	0.25	2.49	5.07	3.02	2.16	0.28	760	2702	572	95.46	4.5
kuw3plag3inclc1	30×30	57.89	1.24	14.13	8.70	0.22	2.10	4.73	2.96	2.40	0.27	944	3062	454	95.08	4.9
	Average	58.75	1.16	14.18	7.92	0.21	2.00	4.59	3.07	2.45	0.27	685	2508	501	94.96	5.0
	1σ SD	1.39	0.14	0.23	1.26	0.03	0.38	0.40	0.10	0.24	0.01	207	457	55	0.48	0.5
KUWPFD	Basaltic andesite glass inclusions in clinopyroxene host															
Label	size (μm)	SiO_2	TiO_2	Al_2O_3	FeO*	MnO	MgO	CaO	Na_2O	K_2O	$P_2O_{>5}$	S	Cl	F	Total	VBD
kuw1cpx1inclb	40×40	53.53	0.99	17.04	9.00	0.17	2.63	6.47	3.04	1.42	0.24	1081	1009	189	94.75	5.3
kuw1cpx1inclc	40×30	52.79	0.97	16.40	10.25	0.17	3.40	7.33	2.78	1.24	0.24	1110	1318	366	95.85	4.1
kuw1cpx1incld	30×20	53.86	1.20	17.15	9.71	0.19	2.39	6.43	2.93	1.32	0.27	1421	1238	211	95.73	4.3
kuw1cpx1incle	70×70 irreg.	52.82	0.94	16.09	10.66	0.18	3.23	7.62	3.05	1.30	0.28	1108	1172	495	96.44	3.6
	Average	53.25	1.03	16.67	9.91	0.18	2.91	6.96	2.95	1.32	0.26	1180	1184	315	95.69	4.3
	1σ SD	0.53	0.12	0.51	0.72	0.01	0.48	0.60	0.13	0.08	0.02	161	131	143	0.70	0.7
KUWPFD	Basaltic andesite glass inclusions in plagioclase host															
kuw3plag8incla1	42×35	52.07	1.01	13.81	11.43	0.21	4.60	7.39	2.63	1.52	0.22	1021	1267	429	95.16	4.8
kuw1plag5incla1	73×51	52.16	1.03	14.91	10.83	0.24	4.27	7.94	2.44	1.30	0.23	900	1105	393	95.57	4.4
kuw1plag5inclb	32×32	53.41	0.74	13.95	10.39	0.17	4.19	7.52	2.48	1.47	0.30	663	1055	449	94.82	5.2
kuw1plag5incle	35×43	52.07	1.26	12.45	12.09	0.26	4.97	7.60	2.50	1.41	0.25	1234	1248	241	95.12	4.9
kuw1plag6incla2	60×60	52.09	1.02	15.41	10.46	0.23	3.92	8.73	3.27	1.13	0.27	1107	1272	328	96.80	3.2
	Average	52.36	1.01	14.11	11.04	0.22	4.39	7.83	2.66	1.36	0.25	985	1189	368	95.50	4.5
	1σ SD	0.59	0.18	1.14	0.72	0.03	0.40	0.54	0.35	0.16	0.03	217	102	85	0.78	0.8

Table 5 (continued)

Label	Size (μm)	SiO_2	TiO_2	Al_2O_3	FeO*	MnO	MgO	CaO	Na_2O	K_2O	P_2O_5	S	Cl	F	Total	VBD
KUWPFD	Basaltic andesite glass inclusions in all host minerals.															
	Average	52.75	1.02	15.24	10.54	0.20	3.73	7.45	2.79	1.34	0.26	1072	1187	345	95.58	4.4
	1σ SD	0.71	0.15	1.60	0.90	0.04	0.88	0.70	0.30	0.12	0.03	210	108	110	0.70	0.7
KUWPFD	Basalt glass inclusions in plagioclase host															
Label	Size (μm)	SiO_2	TiO_2	Al_2O_3	FeO*	MnO	MgO	CaO	Na_2O	K_2O	$P_{2>}0_5$	S	Cl	F	Total	VBD
kuw1plag2inclc1	69×75	50.77	1.13	13.37	11.49	0.28	4.82	9.20	1.96	0.70	0.26	1163	1107	481	94.25	5.7
kuw1plag2incle1	45×50	50.43	1.12	13.27	12.54	0.27	4.99	7.98	1.77	1.00	0.25	1331	1520	546	93.98	6.0
	Average	50.60	1.13	13.32	12.02	0.28	4.91	8.59	1.87	0.85	0.26	1247	1314	514	94.12	5.9
	1σ SD	0.24	0.01	0.07	0.74	0.00	0.12	0.86	0.13	0.22	0.01	119	292	46	0.20	0.2
KUWPFD	Basalt glass inclusion in olivine host															
kuw3ol1incla1	10×10	48.49	0.97	18.26	10.98	0.21	6.97	7.84	1.15	0.97	0.23	897	1048	103	96.28	3.7
KUWJLB	Dacite glass inclusions in clinopyroxene host															
Label	Size (μm)	SiO_2	TiO_2	Al_2O_3	FeO*	MnO	MgO	CaO	Na_2O	K_2O	P_2O_5	S	Cl	F	Total	VBD
hd51cpx1inclb	21×30	66.47	0.52	13.56	4.22	0.11	0.96	3.23	3.78	2.77	0.13	254	1893	526	96.01	4.0
hd51cpx6incla	28×30	67.07	0.73	14.82	3.91	0.05	0.46	2.16	3.67	3.27	0.23	280	1974	615	96.64	3.4
hd52cpx10incla	25×25	63.70	0.69	15.20	5.88	0.13	0.40	3.20	4.26	2.90	0.27	488	1677	451	96.89	3.1
hd52cpxxincla	40×40	66.77	0.72	14.95	3.61	0.14	0.39	2.90	4.21	3.12	0.25	381	2088	698	97.37	2.6
	Average	66.00	0.66	14.63	4.41	0.10	0.55	2.87	3.98	3.02	0.22	351	1908	573	96.73	3.3
	1σ SD	1.55	0.10	0.73	1.01	0.04	0.27	0.50	0.30	0.22	0.06	107	174	107	0.57	0.6
KUWJLB	Dacite glass inclusion in plagioclase host															
hd52plag3incla	NR	66.25	0.46	14.37	4.31	0.17	0.84	3.73	4.34	3.51	0.14	NA	NA	NA	98.12	NA
KUWJLB	Dacite glass inclusions in all host minerals.															
	Average	66.05	0.62	14.58	4.39	0.12	0.61	3.04	4.05	3.11	0.20	351	1908	573	97.01	3.3
	1σ SD	1.35	0.13	0.64	0.88	0.05	0.27	0.57	0.30	0.29	0.06	107	174	107	0.79	0.6
KUWJLB	Andesite glass inclusions in clinopyroxene host															
Label	Size (μm)	SiO_2	TiO_2	Al_2O_3	FeO*	MnO	MgO	CaO	Na_2O	K_2O	P_2O_5	S	Cl	F	Total	VBD
hd51cpx2incla	40×80	60.62	0.69	16.64	6.78	0.16	0.90	3.55	4.23	2.25	0.18	622	1365	457	96.23	3.8
hd51cpx2inclb	35×85	58.49	0.68	18.50	6.21	0.19	1.23	4.21	3.88	2.07	0.23	1097	1412	187	95.96	4.0
	Average	59.55	0.69	17.57	6.49	0.18	1.06	3.88	4.06	2.16	0.20	860	1389	322	96.10	3.9
	1σ SD	1.51	0.01	1.32	0.40	0.02	0.23	0.47	0.25	0.13	0.04	336	33	191	0.20	0.2
KUWSF	Basaltic Andesite inclusions in plagioclase host															
Label	Size (μm)	SiO_2	TiO_2	Al_2O_3	FeO*	MnO	MgO	CaO	Na_2O	K_2O	P_2O_5	S	Cl	F	Total	VBD
kuwsfplag1inclb	54×32	52.71	1.30	15.11	10.44	0.21	4.20	8.50	2.70	2.12	0.42	237	429	355	97.81	2.2
kuwsfplag5inclb	45×45	52.13	1.24	14.89	10.21	0.16	4.16	8.08	2.80	2.25	0.44	188	339	494	96.46	3.5
kuwsfplag6incla	30×30	52.54	1.34	13.92	11.95	0.24	4.76	8.03	2.14	2.30	0.40	432	415	431	97.75	2.3
kuwsfplag7incla	14×22	53.78	1.23	12.99	11.30	0.22	4.85	7.44	2.84	2.46	0.36	489	439	396	97.60	2.4
	Average	52.79	1.28	14.23	10.98	0.21	4.49	8.01	2.62	2.28	0.41	337	406	419	97.41	2.6
	1σ SD	0.70	0.05	0.97	0.80	0.03	0.36	0.44	0.33	0.14	0.03	146	45	59	0.64	0.6
KUWSF	Basalt inclusions in plagioclase															
Label	Size (μm)	SiO_2	TiO_2	Al_2O_3	FeO*	MnO	MgO	CaO	Na_2O	K_2O	P_2O_5	S	Cl	F	Total	VBD
kuwsfplag1incla	35×47	51.67	1.20	15.03	11.21	0.21	4.64	8.70	2.93	1.99	0.42	536	416	385	98.13	1.9
kuwsfplag2incla	37×48 irreg.	51.19	1.24	14.88	11.32	0.24	4.51	8.93	2.81	1.94	0.41	598	458	515	97.63	2.4
kuwsfplag2inclb	35×35	51.33	1.21	14.89	11.29	0.23	4.58	8.80	2.71	2.03	0.38	587	400	506	97.60	2.4
kuwsfplag3incla	40×30	51.19	1.34	13.20	12.84	0.22	5.20	9.37	2.66	1.69	0.43	411	248	147	98.22	1.8
kuwsfplag3inclb	135×60 irreg.	50.86	1.28	15.01	11.20	0.21	4.61	8.83	2.94	1.84	0.40	628	416	387	97.32	2.7
kuwsfplag4incla	29×29	51.07	1.12	14.82	11.53	0.19	4.57	8.49	2.69	2.09	0.38	524	435	477	97.09	2.9
kuwsfplag4inclb	34×61	51.35	1.26	14.16	11.37	0.19	4.89	8.03	2.52	2.21	0.38	602	460	327	96.50	3.5

Table 5 (continued)

Label	Size (μm)	SiO_2	TiO_2	Al_2O_3	FeO*	MnO	MgO	CaO	Na_2O	K_2O	P_2O_5	S	Cl	F	Total	VBD
kuwsfplagxincla	74×71	51.36	1.28	14.67	11.50	0.21	4.77	8.56	3.18	2.06	0.40	576	408	466	98.14	1.9
kuwsfplagxinclb	100×70	50.91	1.16	14.85	11.75	0.22	4.64	8.71	2.77	1.77	0.43	598	362	270	97.33	2.7
kuwsfplagxinclc	40×40	51.36	1.24	14.99	11.12	0.23	4.60	8.65	2.85	2.07	0.38	565	398	497	97.64	2.4
kuwsfplagyincla	44×139 irreg.	51.31	1.24	14.43	11.48	0.21	4.77	8.47	2.85	2.16	0.40	660	480	405	97.47	2.5
	Average	51.24	1.23	14.63	11.51	0.21	4.71	8.69	2.81	1.99	0.40	571	407	398	97.55	2.4
	1σ SD	0.23	0.06	0.54	0.48	0.02	0.20	0.33	0.17	0.16	0.02	66	63	114	0.51	0.5

All data reported as wt% oxides except S, Cl, and F which are reported in ppm. The dividing line between dacite and andesite is 63 wt% SiO_2 according to LeBas et al. (1986), however, we grouped glass inclusions with >62.5 wt% SiO_2 as dacite for naming convenience.
*FeO** total iron; VBD (volatiles by difference) is calculated from: 100 wt%−(sum of oxides and volatile elements)
μm micrometers = 10^{-6} m; *NA* not applicable; NR = not reported; *irreg* irregular shape

F, and 4.4±0.7 wt% H_2O (n=9; Table 5). Basaltic andesite glass inclusions in SF average (±1σ) 337±146 ppm S, 406±45 ppm Cl, 419±59 ppm F, and 2.6±0.6 wt% H_2O (n=4; Table 5). Thus, our data identifies two compositionally distinct basaltic andesite melts preserved in glass inclusions in phenocrysts in Kuwae tephra.

Plagioclase phenocrysts containing basaltic glass inclusions are found in both the dacite pumice (PFD) and the basaltic andesite scoria (SF). One basaltic glass inclusion in olivine in PFD was also found. The compositions of the basaltic glass inclusions are distinct in each of these three cases. Although the plagioclase-hosted basaltic glass inclusions in PFD and SF have similar SiO_2 contents (51 wt%), those in PFD have lower alkali and P_2O_5 contents and higher volatile contents compared to those in SF (Fig. 5, Table 5). Basaltic glass inclusions in plagioclase in PFD average (±1σ) 1247±119 ppm S, 1314±292 ppm Cl, 514±46 ppm F, and 5.9±0.2 wt% H_2O (n=2; Table 5, Fig. 6). Again, it is noted that the high H_2O contents indicated are similar to those obtained under experimental conditions with other basaltic andesite melts (Pichavant et al. 2002).

Basaltic glass inclusions in plagioclase in SF average (±1σ) 571±66 ppm S, 407±63 ppm Cl, 398±114 ppm F, and 2.4±0.5 wt% H_2O (n=11; Table 5, Fig. 6). The basaltic glass inclusion hosted by olivine in PFD is compositionally distinct. Compared with the basaltic glass inclusions hosted by plagioclase it has lower silica (48.5 wt% SiO_2) and lower alkali contents, higher MgO and Al_2O_3, and an intermediate volatile content: 897 ppm S, 1048 ppm Cl, 103 ppm F, and 3.7 wt% H_2O (n=1; Table 5, Fig. 6).

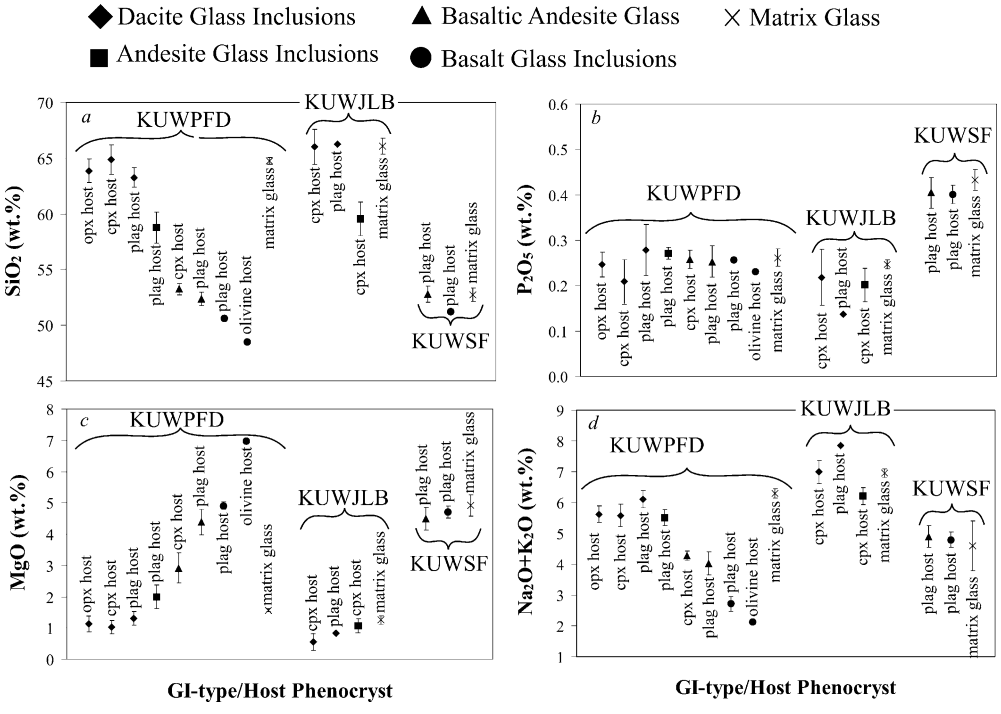

Fig. 5 Averages of selected major element oxide components in glass inclusions and matrix glasses according to host phenocryst and glass composition: **a** SiO_2, **b** P_2O_5, **c** MgO, and **d** Na_2O+K_2O. Host phenocrysts are: orthopyroxene (*opx*), clinopyroxene (*cpx*), plagioclase (*plag*), and olivine. Dacite (*diamonds*), andesite (*squares*), basaltic andesite (*triangles*), and basalt (*circles*) glass inclusions are shown with error bars (1σ). Matrix glasses denoted by X. Data also grouped according to host rock: dacite pumice (KUWPFD), dacite lag breccia (KUWJLB), and basaltic andesite scoria (KUWSF)

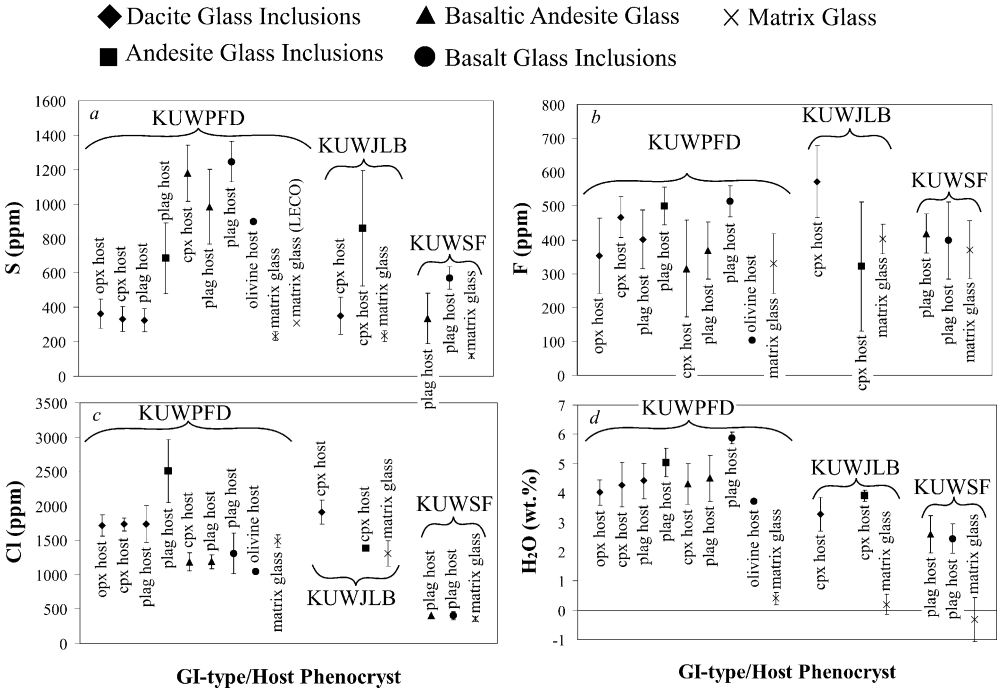

Fig. 6 Averages of volatile components in glass inclusions and matrix glasses according to phenocryst and glass composition: **a** sulfur, **b** fluorine, **c** chlorine, and **d**) H_2O. Host phenocrysts are: orthopyroxene (*opx*), clinopyroxene (*cpx*), plagioclase (*plag*), and olivine. Dacite (*diamonds*), andesite (*squares*), basaltic andesite (*triangles*), and basalt (*circles*) glass inclusions are shown with *error bars* (1σ). Matrix glasses denoted by X. Data also grouped according to host rock: dacite pumice (KUWPFD), dacite lag breccia (KUWJLB), and basaltic andesite scoria (KUWSF)

In summary, our data identifies one compositionally distinct dacite melt, at least five andesite melts, two basaltic andesite melts, and three basaltic melts, all preserved as glass inclusions in phenocrysts in Kuwae tephra. More importantly, most of these compositionally distinct glass inclusions occur within the major dacite batch of erupted magma.

Discussion

Evidence for magma mixing

With a high flux of mafic magma in the region, it is probable that propagating mafic dikes injected and mixed with the pre-eruption Kuwae magma body on multiple occasions. Mixing of basalt, basaltic andesite, and possibly andesite magmas with a continually evolving and crystallizing magma body may explain the mixture of normally zoned, reversely zoned, and oscillatory zoned crystals in the dacite as well as the wide compositional range of the glass inclusions in the phenocrysts in the dacite. Other lines of evidence in support of magma mixing are as follows. First, olivine crystals found in the dacite samples with composition $Fo_{71–74}$ are not in equilibrium with the dacite melt and were likely inherited from an admixed mafic magma. Second, some phenocrysts have dissolved rims or embayments suggestive of crystal-melt disequilibrium. Third, sieve-textured plagioclase common in Kuwae samples may be characteristic of reaction of relatively sodic plagioclase with a more Ca-rich melt (Tsuchiyama 1985). Furthermore, that one episode of magma mixing and co-mingling appears to have played a role in triggering the Kuwae eruption is indicated by the eruption of basaltic andesite scoria immediately prior to the climactic, dominant-volume dacite ignimbrite phase (cf. eruption of Volcán Hudson in 1991, Naranjo et al. 1993).

Sources and masses of volatiles released

Volatiles emitted during the AD 1452 Kuwae eruption most probably originated from a combination of two immediate sources: (1) syn-eruptive degassing of erupted silicate melt (e.g., Devine et al. 1984), and (2) release of a co-existing, volatile-rich fluid phase present in the magma prior to eruption (e.g., Wallace and Gerlach 1994; Wallace 2001; Scaillet et al. 2003). There exists the possibility that the

Table 6 Mimimum volatile emission and aerosol loading estimates for the eruption of Kuwae using the petrologic method

	Volume (km^3)	Mso_2(Tg)	M_{Cl}(Tg)	M_F(Tg)	Theoretical maximum H_2SO_4 aerosols (Tg)
Dacite[a]	30	13	16	6	26
Dacite[b]	60	26	31	12	52

The minimum volatile emission calculations utilize the average volatile contents of co-magmatic glass inclusions and matrix glasses
[a]Uses low estimate for the volume of erupted dacite magma
[b]Uses high estimate for the volume of erupted dacite magma
See text for full explanation

source of volatiles for a separate fluid phase is contributions from more-mafic magmas entering the dominantly dacite magma body. The breakdown of volatile-bearing mineral phases is not considered to be a significant source of volatiles in the Kuwae case since volatile-bearing minerals such as anhydrite, amphibole, and apatite are not found in Kuwae tephra. Sulfide globules are also rare in Kuwae dacite tephra and breakdown products (i.e., spongy Fe-oxide) that would indicate decomposition of sulfide (Larocque et al. 2000) have not been observed. However, the distinct possibility of volatiles from mixed and co-mingled more-mafic melts complicates the picture, which we discuss further below.

Glass inclusions trapped in a variety of phenocrysts in Kuwae tephra, cover a wide range of chemical compositions, and provide important information about the volatile history and evolution of the Kuwae magma body. In some cases, a single phenocryst contains multiple glass inclusions, each with distinctly different chemical compositions, implying that the crystal has been moved around into magmas of different compositions. Which of the many S, Cl, and F values preserved in glass inclusions represents the undegassed, pre-eruptive volatile content of the Kuwae magma? Certainly, the glass inclusions with major-element compositions that are identical to the co-existing matrix glasses most likely preserve volatile contents representative of the "silicate melt" immediately prior to eruption. However, using these data to calculate volatile emission only accounts for degassing from the silicate melt phase of the magma and neglects volatile contributions from other sources such as a separate, volatile-rich fluid phase in the magma, and/or contributions from more-mafic magmas entering the system shortly before, or even during, eruption.

Degassing from dacite melt

The petrologic method for estimating volatile emission from volcanic eruptions involves comparing the volatile contents of (presumed undegassed) glass inclusions within phenocrysts and the volatile contents in (presumed degassed) matrix glasses of the erupted magma. Although, it appears to yield reliable estimates of S emissions from eruptions of mafic magma (e.g., Thordarson et al. 2003; Sharma et al. 2004), the method has been found to yield estimates of volatile emission that are an order of magnitude less than independent estimates for eruptions of silicic magmas (e.g., Pinatubo in 1991; Gerlach et al. 1996). In the discussion below, although we give values for

Table 7 Scenarios for sulfur emission and aerosol loading for the Kuwae eruption based on varying the proportion of volatile-bearing source magmas

Magma source	Basaltic Andesite	Basalt	Total	H_2SO_4 aerosols (Tg) theoretical maximum	H_2SO_4 aerosols (Tg) with 60% efficiency
30 km^3 dacite erupted					
Scenario #1					
Vol. contr. (km^3)	0	56	56	477	286
M_{SO2} (Tg)	0	234	234		
Scenario #2					
Vol. contr. (km^3)	56	0	56	446	268
M_{SO2} (Tg)	219	0	219		
Scenario #3					
Vol. contr. (km^3)	28	28	56	462	277
M_{SO2} (Tg)	110	117	227		
Magma Source	Basaltic Andesite	Basalt	Total	H_2SO_4 aerosols (Tg) Theoretical Maximum	H_2SO_4 aerosols (Tg) with 60% efficiency
60 km^3 dacite erupted					
Scenario #4					
Vol. contr. (km^3)	0	110	110	955	573
M_{SO2} (Tg)	0	469	469		
Scenario #5					
Vol. contr. (km^3)	110	0	110	892	535
M_{SO2} (Tg)	438	0	438		
Scenario #6					
Vol. contr. (km^3)	55	55	110	923	554
M_{SO2} (Tg)	219	234	453		
Average volatile differences for the source magmas used in the calculations above					
ΔS (ppm)	840	898			

In these calculations, we assume the Kuwae magma system was closed to gas loss

Cl and F, we center the discussion around S as this is the main species of interest in stratospheric aerosol formation.

We follow Sharma et al. (2004) by estimating emissions of S, Cl, and F by;

$$M_{S,\,Cl,\,F} = M_v(1 - W_{xtls})(C_{incl} - C_{matrix})/100 \quad (1)$$

where M_S, M_{Cl}, and M_F are the masses of S, Cl, and F in kg (10^9 kg=10^{12} g=1 Tg=1 Megaton), respectively; C_{incl} and C_{matrix} are the concentrations of these elements in glass inclusions ($C_{incl\ S}$, etc.) and matrix glasses ($C_{matrix\ S}$, etc.) in wt%; W_{xtls} is the vesicle-free crystal mass fraction; and M_v is the mass of erupted volcanic deposits in kg. From this, the equivalent mass of sulfur dioxide (SO_2) is:

$$M_{SO2} = 2\left[M_v(1 - W_{xtls})(C_{incl\,S} - C_{matrix\,S})/100\right] \quad (2)$$

A theoretical maximum atmospheric aerosol loading (mass of sulfate aerosols) can be calculated by first multiplying MSO_2 by the ratio of the molecular weight of H_2SO_4 to SO_2 (98:64) and then by 1.33 (assuming that 25% of the mass of sulfate aerosols is water; see Self et al. 1996 and references therein), which together is a factor of ~2.0. However, it has been shown after recent eruptions that not all the SO_2 is converted to sulfate aerosols. For example, about 60% of the Pinatubo SO_2 released was converted into aerosols (Bluth et al. 1992; McCormick et al. 1995). We also use the modifier 0.6 in the calculations that follow to make a first order estimate of the potential sulfate aerosol burden from the Kuwae eruption.

To estimate Kuwae volatile emissions, we first assume that the average volatile content in dacite glass inclusions in the dacite pumice (PFD), regardless of host-phenocryst, represents undegassed samples of the dacite melt that degassed to the atmosphere upon eruption (332 ppm S, 1732 ppm Cl, and 424 ppm F; see Table 5). Matrix glass volatile contents are generally uniform in PFD; we use the average matrix glass volatile contents to represent degassed dacitic melt (232 ppm S, 1492 ppm Cl, and 330 ppm F; Table 4). Volatile differences for co-magmatic glass inclusions (C_{incl}) and matrix glasses (C_{matrix}) in the dacite (PFD) are: S=0.01 wt %, Cl=0.024 wt %, and F=0.009 wt %. For the calculation, W_{xtls}=0.87 (13 vol% crystals; Table 3).

From Eq. (1) and using 7.5×10^{13} to 1.5×10^{14} kg for the mass range of erupted dacite, the calculated S, Cl, and F emissions from the degassing of dacite melt are: 6.5×10^9 kg (6.5 Tg) S, 16 Tg Cl, and 6 Tg F to 13 Tg S, 31 Tg Cl, and 12 Tg F (Table 6). The mass of SO_2 (Eq. 2) would be 13–26 Tg, and, from this, the theoretical maximum sulfate aerosol loading from these erupted masses is 26–52 Tg.

If we use the single co-existing dacite glass inclusion with the highest S content to represent the pre-eruptive S content of the entire dacite magma body (analysis kuw2opx25incla1: 424 ppm (0.042 wt%) S which gives $C_{incl\ S}$ - $C_{matrix\ S}$ of 0.019 wt %), the estimated theoretical maximum H_2SO_4 aerosol loading increases to ~50–~100 Tg. If we use the same 60% aerosol generation efficiency as that which occurred in the Pinatubo eruption cloud (1.2 × mass SO_2), the estimated aerosol mass values fall to 16–31 Tg for the average S concentration case and ~30–~60 Tg for the maximum S concentration case. Thus, as ice core data suggests that a larger aerosol mass was generated by the Kuwae eruption compared to Tambora, these petrologic estimates fall short of the required mass and leave open the possibility that another source of S gas such as a separate S-bearing fluid phase, may have been sequestered in the Kuwae magma. Naturally, the maximum mass and maximum S concentration case comes nearest to providing a realistic amount of S gas from the dacite melt alone.

Degassing from additional sources

If magma accumulated at Kuwae in a magma body that was open to magmatic input but closed or partially-closed to gas escape, then a separate volatile-rich fluid phase is likely to have accumulated. The proposition that large masses of sulfur gases can be generated by mixing of an oxidized silicic magma with a reduced, sulfur-rich mafic magma (Kress 1997) is likely not applicable to the Kuwae eruption. Using experimental work on mafic island arc magmas from Mt. Pelée (Pichavant et al. 2002) as an analogue suggests that, based on the FeO*/MgO ratio of the tephra, Kuwae magmas have an oxygen fugacity in the range ΔNNO+0.5 to ΔNNO+1. This range is within the stability field of sulfide and, furthermore, is consistent with observations of rare sulfide in Kuwae tephra. This lack of the required reduced mafic magma at Kuwae argues against the hypothesis of redox reactions and magma mixing as an origin for the S gas release. We therefore consider two alternative methods to estimate the contribution to volatile emissions from a hypothetical separate fluid phase in Kuwae magma: (1) use volatile data from glass inclusions in phenocrysts in Kuwae tephra to constrain the mass of sulfur that accumulated in the Kuwae magma from a variety of mafic intrusions and (2) use the thermodynamic method of Scaillet et al. (2003) to calculate the mass of SO_2 in Kuwae's separate fluid phase.

We propose that the S, Cl, and F content in the silicate melt phase as well as a possible separate fluid phase present in the Kuwae magma immediately prior to eruption are the end product of a long period of volatile accumulation and transfer from many intrusions of magma into the evolving Kuwae magma body. The relative volumetric proportions of the various S, Cl, and F source reservoirs (intrusions) that contributed to form the final pre-eruptive volatile content of the Kuwae magma reservoir are, however, not known. We assume that the basaltic andesite and/or basalt glass inclusions preserved in the phenocrysts in the dacite samples (PFD and JLB) are representative of parent magma(s) that mixed and differentiated to ultimately form the dacite Kuwae magma body. Furthermore, the average sulfur content found in these diverse mafic glass inclusions can be used to calculate the original sulfur content of the

magma body before it evolved to the dacite magma that ultimately erupted. If, for the present argument, we accept that this quantity of original sulfur was released to the atmosphere during the Kuwae eruption, we need to further assume that: (1) no degassing of volatiles occurred while the Kuwae magma body evolved; (2) there was no removal of sulfur by crystallization of sulfides; (3) all the "excess" volatiles were contained in a separate, exsolved volatile-rich fluid phase within the Kuwae magma body which was released along with the volatiles degassed directly from silicate melt during eruption. This approach provides an upper limit to the mass of sulfur that could have been provided by the magmas present at Kuwae.

Data from glass inclusions are used to construct six scenarios (Table 7) to estimate the volatile emission potentially derived from magma mixing and volatile accumulation in a separate fluid phase. A parent magma volume of 56–110 km^3 is used in the calculations on Table 7 because ~50% (by mass) fractional crystallization will occur during differentiation from the mafic parent magma to ~30–60 km^3 dacite (estimate derived from MELTS; Ghiorso and Sack 1995). The parent magmas which supplied the evolving Kuwae magma body were likely dominated by basalt and basaltic andesite as evidenced by the abundance of basalt to basaltic andesite volcanics in the Kuwae region. If Kuwae erupted only 30 km^3 of dacite (the low end of estimates for erupted volume), mafic parent magmas contained sufficient sulfur to provide >200 Tg SO_2 irrespective of the composition of the mafic parent magmas (basalt, basaltic andesite, or a mixture of the two; Table 7). This mass of SO_2, if erupted, would have been sufficient to generate an aerosol cloud of ~275 Tg H_2SO_4 (assuming 60% efficiency of SO_2 to H_2SO_4 conversion). The mass of sulfur available to generate an H_2SO_4 aerosol cloud if 60 km^3 of dacite were erupted is double that of the 30 km^3 case. In summary, by utilizing the pre-eruptive sulfur content in glass inclusions as a measure of the mass of sulfur that could potentially have accumulated in the Kuwae magma body over time, we can place a maximum bound on the mass of a sulfate aerosol cloud potentially generated by the release of sulfur gases during the Kuwae eruption. This analysis assumes that the Kuwae magma system is closed to sulfur loss. If this assumption is incorrect, our calculations suggest that the evolving Kuwae magma body could have lost up to 50–80% of its sulfur yet still retained sufficient S to generate an H_2SO_4 aerosol cloud with mass >100 Tg.

For comparison, Scaillet et al. (2003) developed a thermodynamic approach to estimate the partitioning of sulfur into a separate, vapor-rich fluid phase based on the composition and oxidation state of the magma. For dacites, the vapor-rich fluid phase has ~72 times the sulfur content of the melt based on experimental evidence (Scaillet et al. 1998). If we use 332 ppm S as the pre-eruptive sulfur content in the dacite silicate melt (as above), this implies that the pre-eruptive sulfur content in a separate fluid phase is 23,900 ppm S (47,800 ppm SO_2=4.78 wt% SO_2). If we assume the separate fluid phase comprises 3.6±1.2 wt% of the Kuwae magma (analogous to Pinatubo; Wallace et al. 1995), then the mass of sulfur in the separate fluid phase would have the range 86–172 Tg SO_2 for the case of 30 km^3 erupted dacite and double that if 60 km^3 of dacite were erupted. These amounts of SO_2 could generate a theoretical maximum H_2SO_4 aerosol mass range from 175–700 Tg for the two magma mass limits used above, or 105–421 Tg at the 60% aerosol conversion rate.

It is clear that the volatile contribution from a separate fluid phase, even the lower estimates, are alone enough to provide the observed amounts of Kuwae acid fall-out. With the addition of what we propose could come from the silicate melt, it seems likely that the Kuwae aerosol mass was derived from both direct degassing from the dacite melt and a component of gas from a sequestered fluid source. Under even modest assumptions for mass of magma erupted and the proportion of separate fluid present, the observed Kuwae magma volatile contents support the hypothesis that this eruption caused the 1453–1457 aerosol event recorded in ice cores. Chlorine releases to the atmosphere could also have been augmented from separate fluid sources within the magma. The most significant conclusion from this study is that it is highly likely that the Kuwae eruption released ≫100 Tg H_2SO_4 aerosols and perhaps released up to a few hundred Tg H_2SO_4 aerosols into the atmosphere in the mid-fifteenth century. The eruption may also have released more SO_2 than the 1783–4 eruption of Laki, Iceland, (~120 Tg; Thordarson et al. 2003).

Potential atmospheric impact of Kuwae aerosols

Evidence for the climatic impact of the eruption of Kuwae comes from tree rings, anomalous weather patterns, and unusual atmospheric optical effects. For example, bristle-cone pines from western US show frost damage in 1453 (LaMarche and Hirschboeck 1984). British oaks show abnormally narrow rings for the period 1453–1455, Chinese cypresses have narrow rings in 1453–1454, and French and Finnish trees were stunted in 1453–1457 (Pang 1993). Briffa et al. (1998) report that tree-ring densities in the Northern Hemisphere show that a strong cooling event occurred in 1453. Although tree-damaging frost events have occurred without coeval volcanic eruptions and large volcanic eruptions have been reported that appeared to have no ill-effects on tree health (LaMarche and Hirschboeck 1984), a direct cause-effect relationship between the eruption of Kuwae and anomalously narrow or frost damaged tree rings in the years 1453–1457 is distinctly possible.

Historians from the Ming Dynasty record strikingly unusual and severe weather in China in 1453–1454. According to Chinese historical records, "nonstop snow damaged wheat crops" in the spring of 1453 (Pang 1993). In addition, "several feet of snow fell in six provinces, 10,000s (of people) froze to death" in the fall of 1453. Also, "it snowed for 40 days south of the Yangtze River, countless died of cold and famine" in early 1454 (Pang 1993). It seems plausible that tropospheric cooling caused

by an immense stratospheric aerosol mass derived from the eruption of Kuwae could be responsible for these unusual meteorological phenomena.

Strange atmospheric optical effects were noted during the siege and fall of Constantinople in April and May 1453. On May 26, "the whole city was blotted out by a thick fog, a phenomenon unknown in those lands in May ... That night, when the fog had lifted ... a strange light played about the dome of the Church of Holy Wisdom ... Lights, too, could be seen from the walls, glimmering in the distant countryside far behind the Turkish camp ... the inhabitants (of the city) believing it to be the reflection of a fire caused by the Turks" (Pang 1993). Stunning red sunsets and other unusual atmospheric optical phenomena were reported following the eruptions of Krakatau in 1883 (e.g., Simkin and Fiske 1983) and Tambora in 1815 (Stothers 1984), the effects being caused by high concentrations of sulfuric acid aerosol droplets suspended in the atmosphere. A direct connection between the fog and optical effects that occurred during the siege of Constantinople and Kuwae eruption in 1452 becomes more plausible.

Conclusions

In the mid-fifteenth century, a large, mainly dacitic volcanic eruption occurred in the present-day Republic of Vanuatu creating the 12×6-km Kuwae submarine caldera. If caldera volume is an adequate proxy for the eruptive volume, then the Kuwae event may have produced between 30 and 60 km^3 (DRE) magma (7.5×10^{13} to 1.5×10^{14} kg, or a magnitude between M6.9–7.2). Utilization of the petrologic method indicates that silicate melt alone degassed 13–26 Tg SO_2, 16–31 Tg Cl, and 6–12 Tg F. This is equivalent to an aerosol cloud with mass 16–31 Tg H_2SO_4. Taking into account possible additional sulfur emitted from a separate, volatile-rich fluid phase, our analysis which used glass inclusion data derived from Kuwae tephra as well as the thermodynamic relations of Scaillet et al. (2003), provides evidence that it is highly likely that atmospheric aerosol loading from the Kuwae eruption was >>100 Tg H_2SO_4. This conclusion corroborates the findings in our companion ice core study (Gao et al. 2006) which shows that the Kuwae eruption produced a single, four-year-long aerosol signal from 1453–1457. A large aerosol mass is consistent with the prolonged ice-core acidity signal.

This study confirms the hypothesis that the Kuwae eruption was a large sulfur producer and is consistent with the contention that Kuwae did produce a globally distributed aerosol cloud. The Kuwae eruption most likely generated the largest atmospheric perturbation from sulfate aerosols of the last seven centuries, even eclipsing the <120 Tg aerosol mass generated by gas release from the 1815 eruption of Tambora (Gao et al. 2006), and possibly Laki in 1783–4 (Thordarson et al. 2003). The Kuwae eruption also probably involved a larger magma mass than Tambora. The 1450s aerosol event was not larger than the unknown eruption that produced large acidity peaks in AD 1258–59. Ice core studies suggest a volcanic event occurred around AD 1257 that generated an aerosol cloud even larger than that of Kuwae. However, the source volcano for this eruption remains unknown (see Oppenheimer 2003 for discussion), and that event may be another case of a "forgotten" caldera, similar to Kuwae which was not recognized as the source of a large eruption until the 1990s.

Acknowledgements JBW was supported by a grant from the Geological Society of America to conduct fieldwork in Vanuatu as well as a University of Hawaii Geology and Geophysics Department graduate fellowship. We thank J.-P. Eissen, M. Monzier, and C. Robin for introducing us to Kuwae caldera. We are particularly grateful to the captain and crew of the schooner *Old Glory* for providing JBW transport and companionship in his return to the Kuwae caldera following an unanticipated boating mishap. The patience and skillful guidance of C. Todd at the University of Hawaii electron microprobe laboratory is much appreciated. B. Scaillet and J. Stix are thanked for providing helpful reviews of an earlier version of the manuscript.

References

Anderson AT (1974) Chlorine, sulfur, and water in magmas and oceans. Geol Soc Am Bull 85:1485–1492

Barsdell M, Berry R (1990) The petrology and geochemistry of western Epi. J Petrol 31:747–777

Bekki S (1995) Oxidation of volcanic SO_2: a sink for stratospheric OH and H_2O. Geophys Res Lett 22(8):913–916

Bekki S, Pyle JA, Zhong W, Toumi R, Haigh JD, Pyle DM (1996) The role of microphysical and chemical processes in prolonging the climate forcing of the Toba eruption. Geophys Res Lett 23(19):2669–2672

Bluth GJS, Doiron SD, Schnetzler CC, Krueger AJ, Walter LS (1992) Global tracking of the SO_2 clouds from the June, 1991 Mount Pinatubo eruptions. Geophys Res Lett 19(2):151–154

Briffa KR, Jones PD, Schweingruber FH, Osborn TJ (1998) Influence of volcanic eruptions on Northern Hemisphere summer temperature over the past 600 years. Nature 393:450–455

Crawford AJ, Green HG, Exon NF (1988) Geology, petrology, and geochemistry of submarine volcanoes around Epi island, New Hebrides island arc. In: Green HG,Wong FL (eds) Geology and offshore resources of Pacific island arcs - Vanuatu region. Earth Science Series, Circum-Pacific Council for Energy and Mineral Resources, Houston, pp 301–327

Delmas RJ, Kirchner S, Palais JM, Petit JR (1992) 1,000 years of explosive volcanism recorded at the South Pole. Tellus 44: 335–350

Devine JD, Sigurdsson H, Davis AN, Self S (1984) Estimates of sulfur and chlorine yield to the atmosphere from volcanic eruptions and potential climatic effects. J Geophys Res 89 (B7):6309–6325

Devine JD, Gardner JE, Brack HP, Layne GD, Rutherford MJ (1995) Comparison of microanalytical methods for estimating H_2O contents of silicic volcanic glasses. Amer Mineral 80:319–328

Eggins SM (1993) Origin and differentiation of picritic arc magmas, Ambae (Aoba), Vanuatu. Cont Mineral Petrol 114:79–100

Gao C, Robock A, Self S, Witter JB, Steffenson JP, Clausen HB, Siggaard-Andersen M-L, Johnsen S, Mayewski PA, Ammann C (2006) The 1452 or 1453 A.D. Kuwae eruption signal derived from multiple ice core records: greatest volcanic sulfate event of the past 700 years. J Geophys Res (in press)

Gerlach TM, Westrich HR, Symonds RB (1996) Preeruption vapor in magma of the climactic Mount Pinatubo eruption: source of the giant stratospheric sulfur dioxide cloud. In: Newhall CG, Punongbayan RS (eds) Fire and mud: eruptions and lahars of Mount Pinatubo, Philippines. PHIVOLCS, Quezon City, Univ Washington Press, Seattle, pp 415–433

Ghiorso MS, Sack RO (1995) Chemical mass transfer in magmatic processes. IV. A revised and internally consistent thermodynamic model for the interpolation and extrapolation of liquid-solid equilibria in magmatic systems at elevated temperatures and pressures. Contr Mineral Petrol 119:197–212

Kress V (1997) Magma mixing as a source for Pinatubo sulfur. Nature 389:591–593

LaMarche VC, Hirschboeck KK (1984) Frost rings in trees as records of major volcanic eruptions. Nature 307:121–126

Larocque ACL, Stimac JA, Keith JD, Huminicki MAE (2000) Evidence for open-system behavior in immiscible Fe-S-O liquids in silicate magmas: implications for contributions of metals and sulfur to ore-forming fluids. Canad Mineral 38:1233–1249

LeBas MJ, LeMaitre RW, Streckeisen AL, Zanettin B (1986) A chemical classification of volcanic rocks based on the total alkali-silica diagram. J Petrol 27:745–750

Mason BG, Pyle DM, Oppenheimer C (2004) The size and frequency of the largest explosive eruptions on Earth. Bull Volcanol 66:735–748

McCormick PM, Thomason LW, Trepte CR (1995) Atmospheric effects of the Mt. Pinatubo eruption. Nature 373:399–404

Monzier M, Robin C, Eissen J-P (1994) Kuwae (~1452 A.D.): the forgotten caldera. J Volcanol Geotherm Res 59:207–218

Naranjo JA, Moreno H, Banks NG (1993) La erupcion del Volcán Hudson en 1991 (46° S), Region XI, Aisén, Chile. Boletín No. 44, Servicio Nacional de Geología y Minería, Santiago Chile

Norrish K, Hutton JT (1969) An accurate X-ray spectrographic method for the analysis of a wide range of geological samples. Geochim Cosmochim Acta 33:431–453

Oppenheimer C (2003) Ice core and paleoclimatic evidence for the timing and nature of the great mid-13th century volcanic eruption. Int J Climatol 23:417–426

Pang KD (1993) Climatic impact of the mid-fifteenth century Kuwae caldera formation, as reconstructed from historical and proxy data. Eos Trans AGU 74(106)

Petrochevsky WA (1949) A contribution to the knowledge of the G. Tambora (Sumbawa). Tijdschr K Ned Aardrijkskd 66:688–703

Pichavant M, Martel C, Bourdier J-L, Scaillet B (2002) Physical conditions, structure, and dynamics of a zoned magma chamber: Mount Pelée (Martinique, Lesser Antilles Arc). J Geophys Res 107:B52093. DOI 10.1029/2001JB000315

Robin C, Eissen J-P, Monzier M (1993) Giant tuff cone and 12-km-wide associated caldera at Ambrym Volcano (Vanuatu, New Hebrides Arc). J Volcanol Geotherm Res 55:225–238

Robin C, Eissen J-P, Monzier M (1994a) Ignimbrites of basaltic andesite and andesite compositions from Tanna, New Hebrides Arc. Bull Volcanol 56:10–22

Robin C, Monzier M, Eissen J-P (1994b) Formation of the mid-fifteenth century Kuwae caldera (Vanuatu) by an initial hydroclastic and subsequent ignimbritic eruption. Bull Volcanol 56:170–183

Robin C, Eissen J-P, Monzier M (1995) Mafic pyroclastic flows at Santa Maria (Gaua) Volcano, Vanuatu; the caldera formation problem in mainly mafic island arc volcanoes. Terra Nova 7:436–443

Robinson BW, Graham J (1992) Advances in electron microprobe trace-element analysis. J Comput-Assist Microsc 4:263–265

Robock A (2000) Volcanic eruptions and climate. Rev Geophys 38:191–219

Savarino J, Bekki S, Cole-Dai J, Thiemens MH (2003) Evidence from sulfate mass independent oxygen isotopic compositions of dramatic changes in atmospheric oxidation following massive volcanic eruptions. J Geophys Res 108:D214671. DOI 10.1029/2003JD003737

Scaillet B, Evans BW (1999) The 15 June 1991 eruption of mount pinatubo. I. Phase equilibria and pre-eruption P-T-fO_2-fH_2O conditions of the dacite magma. J Petrol 40(3):381–411

Scaillet B, Clemente B, Evans BW, Pichavant M (1998) Redox control of sulfur degassing in silicic magmas. J Geophys Res 103(B10):23937–23950

Scaillet B, Luhr J, Carroll MR (2003) Petrological and volcanological constraints on volcanic sulfur emissions to the atmosphere. In: Robock A, Oppenheimer C (eds) Volcanism and the earth's atmosphere. AGU Geophys Monogr 139:11–40

Self S, Zhao J-X, Holasek RE, Torres RC, King AJ (1996) The atmospheric impact of the 1991 Mount Pinatubo eruption. In: Newhall CG, Punongbayan RS (eds) Fire and mud, eruptions and lahars of Mount Pinatubo, Philippines. PHIVOLCS, Quezon City, Univ Washington Press, Seattle, pp 1089–1115

Self S, Gertisser R, Thordarson T, Rampino MR, Wolff JA (2004) Magma volume, volatile emissions, and stratospheric aerosols from the 1815 eruption of Tambora. Geophys Res Lett 31: L20608. DOI 10.1029/2004GL020925

Sharma K, Blake S, Self S, Krueger AJ (2004) SO_2 emissions from basaltic eruptions and the excess sulfur issue. Geophys Res Lett 31:L13612. DOI 10.1029/2004GL019688

Simarski LT (1996) Constantinople's volcanic twilight. Aramco World, Nov–Dec:9–13

Simkin T, Fiske RS (1983) Krakatau 1883 - the volcanic eruption and its effects. Smithsonian Institution Press, Washington, DC, pp 464

Sisson TW, Layne GD (1993) H_2O in basalt and basaltic andesite glass inclusions from four subduction-related volcanoes. Earth Planet Sci Lett 117:619–635

Smith RT, Houghton BF (1995) Vent migration and changing eruptive style during the 1800a Taupo eruption: new evidence from the Hatepe and Rotongaio phreatoplinian ashes. Bull Volcanol 57:432–439

Stothers RB (1984) The great Tambora eruption in 1815 and its aftermath. Science 224:1191–1198

Taylor FW, Bevis MG, Schutz BE, Kuang D, Recy J, Calmant S, Charley D, Regnier M, Perin B, Jackson M, Reichenfeld C (1995) Geodetic measurements of convergence at the New Hebrides island arc indicate arc fragmentation caused by an impinging aseismic ridge. Geology 23:1011–1014

Thordarson T, Self S, Oskarsson N, Hulsebosch T (1996) Sulfur, chlorine, and fluorine degassing and atmospheric loading by the 1783–1784 AD Laki (Skaftar Fires) eruption in Iceland. Bull Volcanol 58:205–225

Thordarson T, Self S, Miller JD, Larsen G, Vilmundardottir EG (2003) Sulphur release from flood lava eruptions in the Veidivötn, Grimsvötn, and Katla volcanic systems. In: Oppenheimer C, Pyle DM, Barclay J (eds) Volcanic degassing, Geol Soc Lond Spec Publ 213:103–122

Tsuchiyama A (1985) Dissolution kinetics of plagioclase in the melt of the system diopside-albite-anorthite, and origin of dusty plagioclase in andesites. Contrib Min Petrol 89:1–16

Walker GPL (1981) Characteristics of two phreatoplinian ashes, and their water-flushed origin. J Volcanol Geotherm Res 9:395–407

Wallace PJ (2001) Volcanic SO_2 emissions and the abundance and distribution of exsolved gas in magma bodies. J Volcanol Geotherm Res 108:85–106

Wallace PJ, Gerlach TM (1994) Magmatic vapor source for sulfur dioxide released during volcanic eruptions: evidence from Mount Pinatubo. Science 265:497–499

Wallace PJ, Anderson AT Jr, Davis AM (1995) Quantification of pre-eruptive exsolved gas contents in silicic magmas. Nature 377:612–616

Witter JB (1997) Volatile emissions and potential climatic impact of the Great Kuwae (Vanuatu) Eruption of ~1452–3 A.D. MS Thesis, University of Hawaii at Manoa, Honolulu

Zielinski GA (1995) Stratospheric loading and optical depth estimates of explosive volcanism over the last 2,100 years derived from the Greenland Ice Sheet Project 2 ice core. J Geophys Res 100:20937–20957